COLORIMETRIC INVESTIGATION OF THE ANTIFERROMAGNETIC TRANSITION IN $NiCl_2 \cdot 6H_2O$

by

William Lewis Johnson

United States Naval Postgraduate School

THESIS

CALORIMETRIC INVESTIGATION

OF THE

ANTIFERROMAGNETIC TRANSITION IN $NiCl_2 \cdot 6H_2O$

by

William Lewis Johnson

December 1969

Calorimetric Investigation of the Antiferromagnetic Transition in $NiCl_2 \cdot 6H_2O$

by

William Lewis Johnson
B.A., University of Southern Mississippi, 1962
M.S., Naval Postgraduate School, 1966

Submitted in partial fulfillment of the
requirements for the degree of

DOCTOR OF PHILOSOPHY

from the

NAVAL POSTGRADUATE SCHOOL
December 1969

ABSTRACT

The results of measurements of the specific heat of nickel chloride hexahydrate in zero and various applied fields are presented. The specific heats of two single-crystal samples were determined in zero field between 4.3 and 5.8 K with temperature resolution of 10^{-6}K. The functional form of the specific heat near the Néel temperature is determined and compared with theoretical predictions. The specific heat maximum of both crystals is found to be rounded over several millidegrees. This non-ideal behavior is analyzed in terms of a complex transition temperature, the imaginary part of which is related to crystalline imperfections. Using data outside the rounded region, it is concluded that the Néel temperature of a perfect crystal would be 5.3475 $\pm$ .001 K. The effect of magnetic fields applied along the easy axis on the specific heat peak was investigated. The peak was found to be slightly broadened by the field, and occurred at lower temperatures. The boundary between antiferromagnetic and paramagnetic phases was determined for fields to 20 kilo-oersteds.

TABLE OF CONTENTS

LIST OF TABLES

LIST OF FIGURES

FIGURE

ACKNOWLEDGMENTS

I would like to express appreciation to the many who helped in this work. Special thanks go to three persons whose patient assistance far exceeded the call of duty. Professor William Reese gave advice, encouragement, and guidance to every phase of the experiment. Lyn F. May provided help in overcoming innumerable impasses in equipment construction and operation. My wife, Pat, did most of the computer programming, besides performing the normal wifely chores of typing, proofreading, etc.

I. INTRODUCTION

This dissertation describes the results of an experimental study of the specific heat of nickel chloride hexahydrate ($NiCl_2 \cdot 6H_2O$), a material which undergoes a phase transition from the paramagnetic to antiferromagnetic state near 5.34 K. The specific heat rises sharply near the transition temperature, but there is no latent heat involved. Such a transition is called a "higher order" transition since there is no discontinuity in the free energy (a necessary condition for any phase transition) or in any of its first derivatives; the higher order derivatives, however, may have a discontinuity. For example, a second order transition may have a discontinuity in the specific heat. Many materials undergo higher-order transitions; just a few examples are ferroelectrics, liquid helium, binary alloys, and a gas near its critical point. The shape of the heat capacity peak appears strikingly similar for these transitions; however, differences among them become apparent when investigated with high temperature resolution. The fact that a wide variety of transitions behave somewhat alike is all the more interesting when one realizes the vast differences in the nature of the interactions that cause the transitions. Although this experiment investigated a particular type of transition, the results may have application to other critical point phenomena.

Theoretical progress in understanding magnetic phase transitions has been made on two fronts. One type of theory emphasizes the details of the interaction, and a calculation of thermodynamic

quantities follows from statistical mechanical methods. In another class are general phenomenological theories applicable to a variety of types of phase transitions. In the next section, certain elements of these theories which are pertinent to this experiment are described. Following this, the properties of $NiCl_2 \cdot 6H_2O$ are discussed, and the experimental apparatus and procedure are explained. Data is presented showing the nature of the transition in applied fields up to 20 kilo-oersteds.

II. THEORY OF ANTIFERROMAGNETIC PHASE TRANSITIONS

A. BACKGROUND

All theories of antiferromagnetism in insulators start with the Heisenberg-Dirac Hamiltonian for the crystal:

$$\mathcal{H} = -2 \sum_{i<i} J_{ij} \vec{S}_i \cdot \vec{S}_j - g \mu_B \vec{H} \cdot \sum_i \vec{S}_i , \qquad (1)$$

where i and j designate the magnetic ions, the $\vec{S}$ are the spin operators, and $\vec{H}$ is the applied field. In many crystals the orbital momentum is quenched, so g is about two. The J_{ij} are called direct exchange integrals; if J_{ij} is negative, anti-parallel alignment between the i and j electron spins produces the lowest energy state. This interaction between spins arises because of the requirement that the wave functions for any two electrons in the crystal be antisymmetric. It is not obvious for real antiferromagnets that this Hamiltonian is a proper approximation because the exchange integral depends on the amount of overlap of the wave functions, and, in hydrated salts of iron-group atoms (and most other antiferromagnetic salts), the magnetic ions are much too far apart for there to be an appreciable overlap of the atomic d-shell wave functions. In these salts the magnetic ions are separated by non-magnetic atoms, for example, chlorine or oxygen. The proper wave functions for the d-shell electrons of the magnetic ions can be shown to be an admixture of isolated, single-atom, wave functions of the magnetic and non-magnetic electrons (Anderson 63 a,b). Each of these

electrons can still be thought of as having its own perturbed wave function, which can be calculated from Hartree-Fock equations. These new wave functions overlap considerably and can create an antiparallel state with lowest energy. Such an interaction via an intermediate non-magnetic atom is called superexchange. It can be shown that the superexchange interaction can be described with a Hamiltonian retaining the familiar Heisenberg-Dirac form (Anderson 63 b).

In addition to the exchange term in the Hamiltonian there are other interactions between the spins, for example, pure dipole-dipole magnetic interactions. These terms are anisotropic and are usually accounted for by introducing an effective magnetic field acting in the preferred direction.

The ideal procedure to follow would be to use the Hamiltonian to calculate the partition function from

$$Z = \text{Trace } (\exp - \mathcal{H}/kT).$$

Using the partition function, such thermodynamic quantities as specific heat or susceptibility can be calculated. For example, the specific heat is given by

$$C = \frac{\partial}{\partial T}\left[kT^2 \frac{\partial}{\partial T} (\ell n\ Z) \right].$$

This exact approach has been usefully applied in the high-temperature and low temperature limits. At high temperatures, Z can be expanded in a series of powers of 1/T. Evaluation of the series involves calculations of mean values of the energy, for which exact wave functions are not necessary. In the low-temperature limit, the deviations of the system from its ground

state can be represented by low-energy excitations called spin waves. Neither of these limits can be successfully extrapolated to give precise information about the phase transition; however, the series expansions have been extensively exploited in an effort to obtain estimates of the critical point behavior (Domb 65).

In order to allow an investigation of the phase transition itself, the basic Hamiltonian must be simplified. Two types of approximations are made in the Hamiltonian to make it tractable at the transition temperature. One is the mean-field approximation, the other is the Ising model approximation. The following sections describe predictions which these models make about the specific heat and about the effect of applied fields on the transition.

B. MEAN FIELD THEORY

This theory makes several approximations to equation 1. The simplest picture assumes that there are two interpenetrating sub-lattices, A and B; that an A atom has only B atoms as nearest neighbors and vice versa; and that an atom only interacts with its nearest neighbors. Then the Hamilitonian can be written as:

$$\mathcal{H} = -2J \sum_{i=1}^{N} \vec{S}_i \cdot \sum_{j=1}^{z} \vec{S}_j + g\mu_B \vec{H} \cdot \sum_{i=1}^{N} \vec{S}_i$$

where z represents the number of nearest neighbors, and N the total number of atoms. It is now assumed that each spin can be replaced by an average value: All spins on A sites having

the average value $\langle \vec{S}_A \rangle$ and those on B sites, $\langle \vec{S}_B \rangle$, so that

$$\mathcal{H} = -2J\left[\sum_{i=1}^{N/2} \vec{S}_i \cdot z \langle \vec{S}_A \rangle + \sum_{i=1}^{N/2} \vec{S}_i \cdot z \langle \vec{S}_B \rangle\right] + g\mu_B \vec{H} \cdot \sum_{i=1}^{N} \vec{S}_i .$$

Next two effective fields are defined which act on atoms in each sublattice. The field acting on an A atom is

$$\vec{H}_A = \vec{H} + \frac{2zJ}{g\mu_B} \langle \vec{S}_B \rangle ,$$

and on a B atom

$$\vec{H}_B = \vec{H} + \frac{2zJ}{g\mu_B} \langle \vec{S}_A \rangle .$$

$\langle \vec{S}_A \rangle$ and $\langle \vec{S}_B \rangle$ can also be expressed in terms of $\vec{H}_A$ and $\vec{H}_B$ using the Brillouin function. This yields two coupled equations for both sublattices. The external field is set to zero and the temperature that gives non-zero H_A and H_B is found and identified as the transition temperature or Néel temperature. The result is

$$kT_N = \frac{2}{3} J \; z \; S(S+1).$$

The resulting specific heat rises from zero at 0 K to a maximum at T_N of

$$C_{max} = 5/2 \; NR \; \frac{(2S+1)^2 - 1}{(2S+1)^2 + 1}$$

and drops to zero discontinuously at T_N. Thus the transition is second order.

This simplest mean field model has been investigated with an external field applied parallel to the axis of sublattice magnetization (Nagamiya 55). The transition temperature in field H is lowered from the Néel temperature in zero field and is given by the equation

$$\frac{T_N(H)-T_N(0)}{T_N(H)} = -\ 27/720\ \frac{(S+1)^2+S^2}{(S+1)^2}\ \frac{\chi_\perp^{\,2}}{M_s^{\,2}}\ H^2, \qquad (2)$$

where $M_s = \frac{1}{2}Ng\mu_B S$ and $\chi_\perp$ is the susceptibility perpendicular to the axis of magnetization. The transition remains second order for all fields up to a critical field

$$H_C = kT_N/g\mu_B.$$

Above this field there is no antiparallel order. This value of the critical field is to be expected based on the simple argument that the effective field must be related to the transition temperature by

$$g\mu_B H_A \approx kT_N,$$

since at T_N an atom has enough thermal energy to break the order produced by H_A. Hence, at T = 0, in order to break up the antiparallel ordering the external field must cancel the internal field.

The main feature of this model is the assumption that a given atom interacts with its neighbors as if their spin took on the average value. This approximation neglects correlations between spins. If an atom has a given direction for its spin, the

probability that its neighbors have a correlated direction is increased from that given by the average. Although the sublattice magnetization, or long range order, disappears at T_N, some short range order is expected to persist above T_N. This defect in the model can be improved by treating the exchange interaction of a given atom within a cluster of its neighbors exactly and replacing all other interactions by an effective field. This is called the Bethe method. The resulting partition function for such a model is an external field has been evaluated (Ziman 51). There is a second order transition for all fields below the critical field. The specific heat is discontinuous at T_N as in the previous model; but it remains non-zero above T_N; a result true for any approximation that allows for short range order above T_N.

C. ISING MODEL

The Ising model approximates the Hamiltonian by

$$\mathcal{H} = - 2J \sum_{i<j} S_{iz} S_{jz} - g\mu_B H \sum_i S_{iz} .$$

This amounts to assuming that the interaction between spins is highly anisotropic; or alternatively, that the spins are replaced by their time averaged values, since $\bar{S}_x = \bar{S}_y = 0$. This assumption is not compatible with spin waves, thus the Ising model is not accurate at low temperatures. But near the phase transition, the statistical enumeration of states is more important than the precise form of the interaction; so the Ising model predictions are in reasonable agreement with many experiments.

The solution for two dimensional lattices can be carried out exactly (Onsanger 44). For $S = \frac{1}{2}$ the heat capacity goes to infinity at T_N and is given by

$$C = A \ln |T-T_N| .$$

However the predicted value of T_N is lower than that given by simple mean field. When $S = 1$ the specific heat rises more rapidly for $T > T_N$ than for $T < T_N$, but the variation is still logarithmic. (A is larger on the high temperature side of the transition.) In three dimensions the exact solution has not been found, but approximations can be made. One result which has been definitely established is that the "tail" of the specific heat curve is much smaller in three than in two dimensions. The details of the nature of the singularity for three-dimensional arrays are indefinite, but there is evidence that C goes to infinity logarithmically for $T < T_N$, and for $T > T_N$ it diverges as $[(T-T_N)/T_N]^{-\alpha}$, where α is about .2 (Baker 63).

Fisher has solved the two-dimensional Ising model in a magnetic field for a lattice with a square array of magnetic atoms coupled to neighboring non-magnetic atoms (Fisher 60). This arrangement introduces superexchange into the model. While this model appears to be more complicated than a simple square lattice, its partition function is an applied field can be related to the standard one for a square lattice in zero field. It thus provides the only Ising model structure which has yielded to an exact solution in a field. For this model the heat capacity goes to infinity logarithmically at T_N, and T_N goes down as

H goes up. For $S = \frac{1}{2}$, and for small H, the result for the phase boundary is

$$\frac{T_N(H) - T_N(0)}{T_N(0)} = - .347\left(\frac{g^2\mu_B^2}{2J^2}\right)H^2 \quad . \tag{3}$$

Numerical calculations on cubic Ising model lattices in applied fields have been carried out (Bienenstock 66); the variation of the transition temperature with field for a cubic lattice is given by

$$\frac{T_N(H)}{T_N(0)} = \left[1 - (H/H_c)^2\right]^{.35}$$

where $H_c = z|J|/g\mu_B$.

Real transitions have characteristics which are reminiscent of predictions of the Ising model results. In order to make comparisons between experiment and theory, critical point exponents are introduced. These exponents characterize singularities in measured quantities near the critical point. The specific heat is written as

$$C_+ = A/\alpha\left[\epsilon^{-\alpha} - 1\right] + B \quad \text{for } T > T_N \tag{4a}$$

and

$$C_- = A'/\alpha'\left[\epsilon^{-\alpha'} - 1\right] + B' \quad \text{for } T < T_N \tag{4b}$$

where

$$\epsilon = \left|\frac{T - T_N}{T_N}\right| .$$

These expressions reduce to

$$C_+ = -A \ln \epsilon + B$$

and

$$C_- = -A' \ln \epsilon + B'$$

when α and α' are zero.

D. LANDAU THEORY

The mean field and Ising theories use approximations to the Hamiltonian in order to arrive at predictions for the free energy and thermodynamic observables. Landau theory, on the other hand, begins with an expression for the free energy. This approach may be applied to many types of transitions, with changes only in the pertinent variables. The theory assumes that the free energy is a function of the normal variables: T, H, etc., and also depends on an extensive quantity which is zero in the high temperature phase and non-zero just below the transition temperature. In the general treatment of transitions, this quantity is called the order parameter; specifically, for antiferromagnets it is proportional to the sublattice magnetization, for ferroelectrics it becomes the spontaneous polarization. The theory can then be developed in terms of the order parameter without reference to a particular type of transition.

Designating the order parameter as η, the free energy in zero field is written as

$$\Phi = \Phi_o + A \eta^2 + B \eta^4 + \cdots$$

For symmetry reasons there can be no odd order terms in η, and the fourth order term must be positive for a second order transition. The procedure is to find the value of η which minimizes this free energy expression. There are two solutions corresponding to the two phases: $\eta = 0$ if A is positive, and $\eta = -A/2B$ if A is negative. Since A must change sign at the transition temperature, its simplest form is $A = a(T-T_N)$. Using this form, the specific heat is found to be discontinuous at T_N. In fact, all predictions of this simplest version of Landau theory are in agreement with the simplest mean field theory. It is easy to see why the two are equivalent. In both models the free energy is assumed to depend on the average order parameter. Since the assumptions are basically the same, currently little distinction is made between the two models.

Simple Landau theory predicts no long-range order above T_N, that is, the sublattice magnetization is zero. But it is possible that just above T_N there may be microscopically large regions over which the sublattice magnetization is non-zero. This is the short-range order that is accounted for in mean field theory by inclusion of interactions with clusters of neighbors. In Landau theory the presence of short-range order is described in terms of spatial fluctuations in the order parameter from its average value. To modify the simple Landau theory, a term is introduced into the free-energy density which causes it to be raised if there are spatial variations in the order parameter. This term is usually assumed to take the form $D|\nabla\eta|^2$. Minimization of the total free energy yields a differential equation

which can be solved for η. In one dimension, above T_N, the solution predicts that if, at position x = 0, η has a value of η_o; then at some other position, x,

$$\eta = \eta_o \exp(- x/\ell)$$

where

$$\ell = |D/A|^{\frac{1}{2}} = \left|\frac{D}{a(T-T_N)}\right|^{\frac{1}{2}}$$

(ℓ is called the correlation length). This indicates that as $T \to T_N$, $\ell \to \infty$; that is, the range over which a deviation of η from its average value produces a correlated change grows as T approaches the transition temperature. Similarily, far below the transition, it is energetically unfavorable for the order parameter to deviate from the average; but as T_N is approached from below the energy cost of a fluctuation decreases and ℓ diverges.

From the viewpoint of the previous paragraph, the infinity in the heat capacity is caused by the infinity in the correlation length. This can be put on a firmer base by defining the correlation functions for the order parameter and energy:

$$K_\eta(r,r') = \langle[\eta(r) - \langle\eta(r)\rangle]\,[\eta(r') - \langle\eta(r')\rangle]\rangle$$

$$K_E(r,r') = \langle[E(r) - \langle E(r)\rangle]\,[E(r') - \langle E(r')\rangle]\rangle.$$

These functions measure how much the deviation in a quantity at one point from its average is correlated to the deviation at another point. One can envoke a theorem in statistical mechanics

to relate the energy correlation function to the heat capacity:

$$C = 1/kT^2 \iint d^3r \; d^3r' \; K_E(r,r').$$

The problem of calculating measured thermodynamic quantities reduces to that of finding the correlation functions for sublattice magnetization and energy. Differential equations can be developed and solved for the correlation functions. The results depend on the dimensionality of the system, but generally the functions decrease exponentially with characteristic length ℓ. Calculations which take correlations into account yield an infinity in the specific heat, and the high temperature side of the singularity has a tail, similar to that produced in the mean field theory when short range interactions are treated exactly.

E. CRYSTAL INHOMOGENEITIES

From the previous equation relating C to $K_E(r,r')$ it is seen that one integrates K_E over the volume of the crystal to get the heat capacity. If the crystal is homogeneous and infinite, the integral cuts off because of the exponential decay of the integrand. However, very near T_N, K_E is large over an appreciable distance. If this distance is larger than a length characteristic of the imperfections in the lattice, it might be expected that the integration should be cut off at this point. That is, it can be argued that the correlations should not be allowed to extend beyond microcrystalline imperfections. Since the theoretical infinity in C is related to

the infinite correlation length, the experimentally observed rounding in C for many transitions might be caused by such imperfections.

The effect of boundaries and finite size on the transition has been studied by several authors (Maki 69) (Ginzburg 58) (Fisher 67). Maki and Ginzburg expand $\eta(r)$ in a Fourier series with each normal mode having amplitude η_q. Only the long wavelength modes are responsible for the transition, so the free energy is expressed in terms of the amplitudes of these modes. For an infinite crystal the sum is carried out for all wave numbers, q, between 0 and q_{max} where q_{max} is the order of the inverse cell dimension. For small systems the sum over the wavelengths of the modes is cut off at some maximum length corresponding to $q = q_{min}$. An application of this procedure has been made to a film of helium contained between two plates separated a distance d. The superfluid transition temperature is calculated to be lowered by an amount given by $\Delta T_\lambda = - 2 \times 10^{-14}/(d_{cm})^2$ (Ginzburg 58). Using a slightly different form for the free energy expansion the transition is predicted to be lowered by $\Delta T_\lambda = - 1.3 \times 10^{-12}/(d_{cm})^{3/2}$ (Maki 69). Although these predictions make some assumptions which are specialized to helium, it is clear from the calculations that the phenomenon of the lowering of the transition temperature is not dependent on these assumptions, but on the finite extent of the correlations.

The effect of interfacial boundaries and finite sample size on the two-dimensional Ising model has been investigated (Fisher 67). The transition rounding is found to be due to truncation of correlation modes having low wave numbers, as in the above Landau calculation. The calculations suggest that the maximum in the specific heat for an inhomogeneous crystal will occur at temperature, T_{max}, lower than T_N, the order of magnitude of the shift given by

$$\frac{T_N - T_{max}}{T_N} \approx \frac{1}{n} , \qquad (5)$$

where n is the number of atoms between adjacent boundaries. It is suggested that instead of using $\epsilon = (T-T_N)/T_N$ in the expression for C (equation 4), one should use

$$\epsilon^* = \left\{ \left(\frac{T - T_{max}}{T_N} \right)^2 + \frac{\tau^2}{T_N^2} \right\}^{\frac{1}{2}} . \qquad (6)$$

Such a temperature dependence produces a specific heat maximum at T_{max} with size determined by τ. The transition is also smeared out over a width determined by τ. τ is estimated for two-dimensional lattices to be the same order of magnitude as the shift, while for three dimensions the width may be smaller than the shift.

More generally, it has been pointed out that a phase transition can be thought of in terms of zeros of the partition function (Fisher 65). These zeros occur at certain values of T, but T can be viewed as a complex variable. For a finite sample the zeros lie off the real temperature axis and close on the real axis as the number of particles goes to infinity. Thus, the

transition in a finite sample is pictured as occuring at a complex temperature, $T = T_{max} + i\tau$, and the quantity $(T_{max}^2 + \tau^2)^{\frac{1}{2}}$ becomes the proper variable to use in analyzing the rounding of the transition. A similar procedure has been used successfully in analyzing the rounded specific heat maximum of a ferromagnet in an applied field (Teaney 68).

III. THE NATURE OF $NiCl_2 \cdot 6H_2O$

A. CRYSTAL STRUCTURE

Nickel chloride hexahydrate ($NiCl_2 \cdot 6H_2O$) is a green monoclinic crystal with two molecules per unit cell. Its molecular weight is 237.71 grams/mole, and the density at room temperature is 1.92 gm/cm^3. The space group is C_2/m and the lattice parameters are a = 10.23Å, b = 7.05Å, c = 6.57Å, and $\beta = 122^\circ$, 10' (the angle between a and c axes) (Mizuno 61). This crystal structure has been confirmed at 4.2 K, and the lattice parameters are only slightly smaller (Kleinberg 69). Each nickel atom is surrounded by a square of 4 oxygens, and two chlorines are on a line perpendicular to the plane of the square. Thus each nickel ion is at the center of a tetragonal bipyramid. Nickel atoms are located at each cell corner and at the center of the faces in the a-b plane. The $NiCl_2 \cdot 4H_2O$ bipyramids are joined together by hydrogen bonds to form two-dimensional layers in the a-b plane. These layers are loosely joined by weaker hydrogen bonds along the c direction. A simplified drawing of this structure is shown in Fig. 1.

B. MAGNETIC PROPERTIES

The Ni^{++} ions have eight 3d-electrons. The ground state of the isolated ion is ^3F, and the crystal-field splitting results in a singlet ground state about 10^4 cm^{-1} below other levels. The crystal field quenches the orbital angular momentum, so the ions have a Lande g-factor of about 2.

The susceptibility of powder (Haseda 57) and single crystal samples (Haseda 59) (Flippen 60) have been measured. χ_b and χ_c, (the susceptibilities measured with the field along the b and c axes) are nearly equal, and temperature independent below 6.2 K. $\chi_{a'}$, measured along the axis perpendicular to c, decreases below 6 K in the manner associated with the parallel susceptibility of an antiferromagnet. Above 6 K all three components are equal indicating an isotropic g-factor. The g-factor was found to be 2.2, and the Weiss temperature was determined to be 10 K (Haseda 59).

The behavior of $\chi_{a'}$ gave rise to the initial interpretation that the a' axis was the axis of sub-lattice magnetization. Recently both neutron diffraction and antiferromagnetic resonance measurements have shown this to be in error. The neutron diffraction results (Kleinberg 67) show that the easy axis is in the a-c plane inclined 10^{o} from the a axis toward the c axis. This data, combined with NMR experiments (Spence 64), give the magnetic structure outlined in Fig. 2.

Antiferromagnetic resonance experiments performed in fields up to 100 kilo-oersteds confirm this structure: the easy axis is found to be 7^{o} from the a axis (Date 67). The effective exchange field was calculated as 86 kilo-oersteds and the anisotropy constants were found. Anisotropy in an antiferromagnet can lead to the phenomena of spin flopping. This occurs if a large field is applied along the easy direction. When the field is applied, the free energy of the system changes by $-\chi_{\|}H^2/2$ if the spins remain antiparallel along the easy axis, and by $-\chi_{\perp}H^2/2$ if they

were to flop at right angles to the easy axis and there were no anisotropy. Since $\chi_\perp > \chi_\parallel$, this would make the perpendicular orientation the ground state. However, there is anisotropy in all antiferromagnets (which is why there is an easy axis). The anisotropy can be described by a constant K, so that the actual change in free energy for the perpendicular alignment becomes $K - \chi_\perp H^2/2$. Therefore it is seen that anisotropy is basic for the retention of the antiferromagnetic state in applied fields. However if H is large enough, so that $K - \chi_\perp H^2/2 \leqq -\chi_\parallel H^2/2$, the perpendicular orientation is preferred. At a critical field given by $H_f^2 = 2K/(\chi_\perp - \chi_\parallel)$, the spins flop perpendicular to the field. H_f can be determined from antiferromagnetic resonance data. For $NiCl_2 \cdot 6H_2O$, H_f is estimated to be 40 kilo-oersteds at 1.5 K (Date 67).

The details of the superexchange linkages in this salt are not clear, but it is probable that the chlorine ions couple the nickel spins (Robinson 60). Its crystallographic two-dimensional layer structure may not be reflected in the magnetic coupling. Inspection of Fig. 2 shows that nearest neighbors in the a-b plane are antiparallel, and there is also antiparallel alignment between corresponding spins in adjacent planes. This arrangement indicates a three-dimensional magnetic structure. The exchange field is large compared to the anisotropy fields so that the Ising model predictions may not be valid.

C. THERMAL PROPERTIES

The specific heat of $NiCl_2 \cdot 6H_2O$ has previously been measured in zero field from 1.4 to 20 K (Robinson 60). This experiment showed the existence of a lambda anomaly at about 5.34 K. The temperature resolution was about .05 K, so that no detailed critical point behavior was obtained. The total entropy gained in the transition was shown to be 9.13 joules/mole-K. This value is in good agreement with the expected value, R ln (2S+1), where S = 1. From the total area under the specific heat curve, an estimate can be made of $z|J|/k$, where J is the exchange integral and z is the number of nearest neighbors. The value was found to be 7.4 K, and if z is taken as 6, $J \approx 1.2k$.

A search for the spin - flop transition in $NiCl_2 \cdot 6H_2O$ has been made in fields up to 10 kilogauss and for temperatures between 1 and 4 K (McElearney 68); no such transition was found. The phase boundary between antiferromagnetic and paramagnetic states was investigated. The Néel temperature was found to change very little with field, however there is considerable scatter in the data.

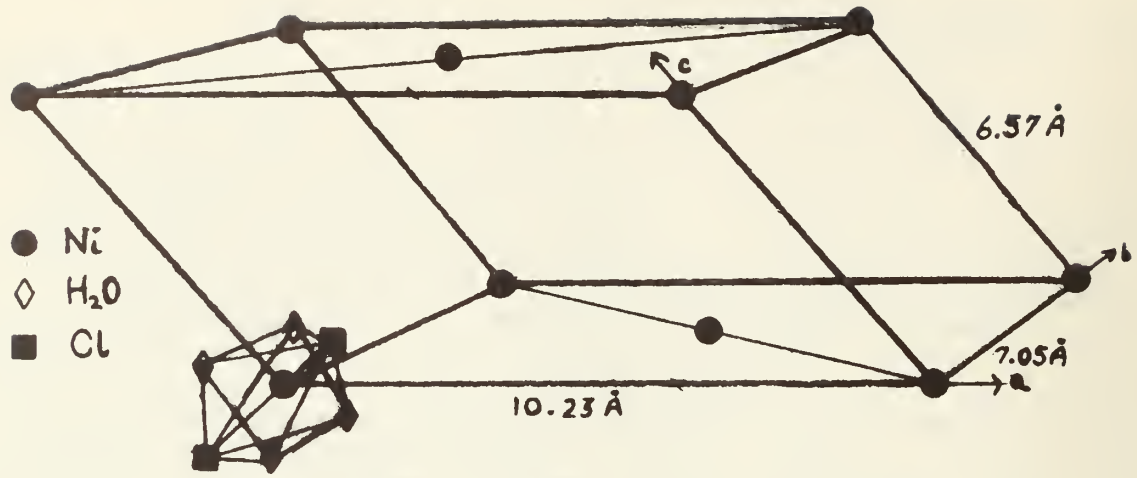

Figure 1: Lattice structure of $NiCl_2 \cdot 6H_2O$

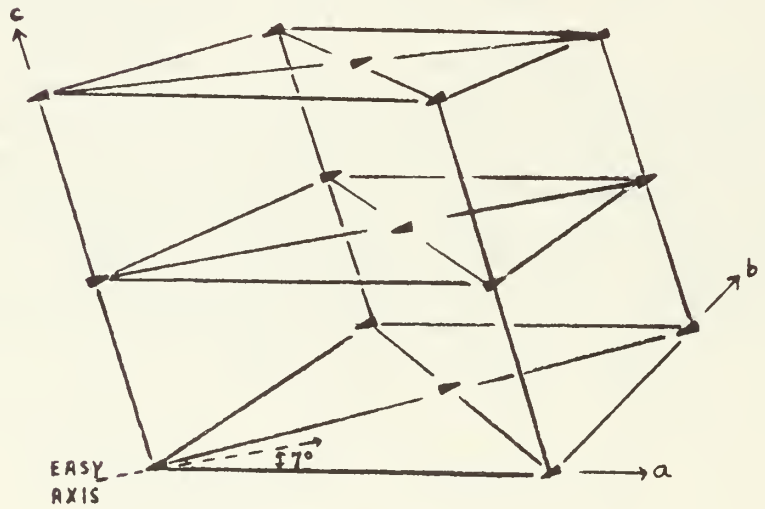

Figure 2: Antiferromagnetic structure

IV. EXPERIMENTAL PROCEDURE

A. CRYOSTAT

The cryostat used for this experiment was designed for applications over the temperature range 1 - 30 K. It allows specific heat measurements to be made under adiabatic conditions in magnetic fields from 0 to 25 kilo-oersteds. The magnetic field is produced by a superconducting solenoid. Because the superconducting magnet performs best when its temperature is 4.2 K, it is necessary to provide a separate pumped helium bath in order to reach lower temperatures.

Figure 3 is a diagram of the lower part of the calorimeter. The sample is suspended by nylon threads from a copper shield; the details of the suspension vary with the size and shape of the sample. In this experiment it was necessary to rotate the sample about a horizontal axis during alignment. The mounting shown allows this to be done. The mounting of the sample is explained in part B.

In order to cool the sample to the bath temperature in a reasonable time, it must be provided with a thermal connection to the bath. This is accomplished using a heat switch. Two jaws mounted on the shield can be opened and closed by a shaft which moves vertically. The shaft is connected to a bellows at the top of the cryostat by a thin wire so that the jaws can be operated external to the cryostat. A copper wire vane extends vertically from the sample to the center of the jaws. When shut,

the indium-coated edges of the jaws grip the wire and provide thermal contact to the shield. An electrical lead is connected to the vane to indicate when the contact is made or broken; a check of the resistance from the vane to the cryostat indicates when contact is made. (Low electrical power must be used to avoid heating the sample and shield when this check is made.)

Surrounding the sample is a shield which is suspended from the low-temperature bath by a brass tube. The shield lid has a heater and a resistance thermometer so that its temperature can be raised and maintained at a constant value above that of the bath. A controller, described in Appendix B, regulates the temperature of the shield to within better than $\pm 10^{-4}$ K of the desired temperature. Also mounted on the shield lid is a terminal circle which provides connections for as many as twenty-two .005" manganin wires which lead to the top of the cryostat, and thence to the electronic equipment in the room.

The calorimeter is evacuated with a diffusion pump connected to the ½ inch inner tube. During an experiment, the pressure in the sample space (as read on an ion gauge in the room) is usually less than 3×10^{-6} Torr. All pumping lines leading to the top of the cryostat have flexible bellows to prevent vibrations from heating the sample. The cryostat and its dewars are mounted on a very heavy wooden structure which is isolated from the floor by sand.

Concentric with the ½ inch pumping line is a 1½ inch tube. The bottom and top ends of these tubes are terminated in such a way that they are completely isolated, that is one may be

evacuated while the other is at atmospheric pressure. Helium can be admitted into the $1\frac{1}{2}$ inch tube through a needle valve, controlled from the room. If experimental work is to be done below 4 K, the needle valve is opened and the inner bath filled. The needle valve is then shut and the inner bath pumped to lower its temperature. Once the helium level falls below the needle-valve opening, the temperature decreases rapidly, since the inner bath is coupled to the four-degree bath only by a length of stainless steel tubing. Three resistors are mounted in the inner bath so that the level can be roughly determined. When the helium reaches the lambda point, superfluid film creep up the walls of the tubing commences; this circulation causes a heat input to the bath which limits the lowest temperature that can be reached. To prevent this circulation, two baffles were soldered into the tubing about one and two inches above the bottom. Once the level gets below these baffles the temperature of the bath falls to its lowest value; and, because the heat into the bath is very small, the liquid helium remains for several hours at about 1.2 K. If the magnet is being used the outer helium bath is kept at 4.2K; but, for experiments which do not use the magnet, the outer bath may also be pumped with a large mechanical pump. If this is done, and if the inner bath is pumped with a diffusion pump, the lowest temperature reached is less than 1 K.

The calorimeter and inner helium bath are surrounded by a brass can which is bolted to the ring containing the needle valve. An O-Ring, formed from indium wire, is wrapped around the lip of

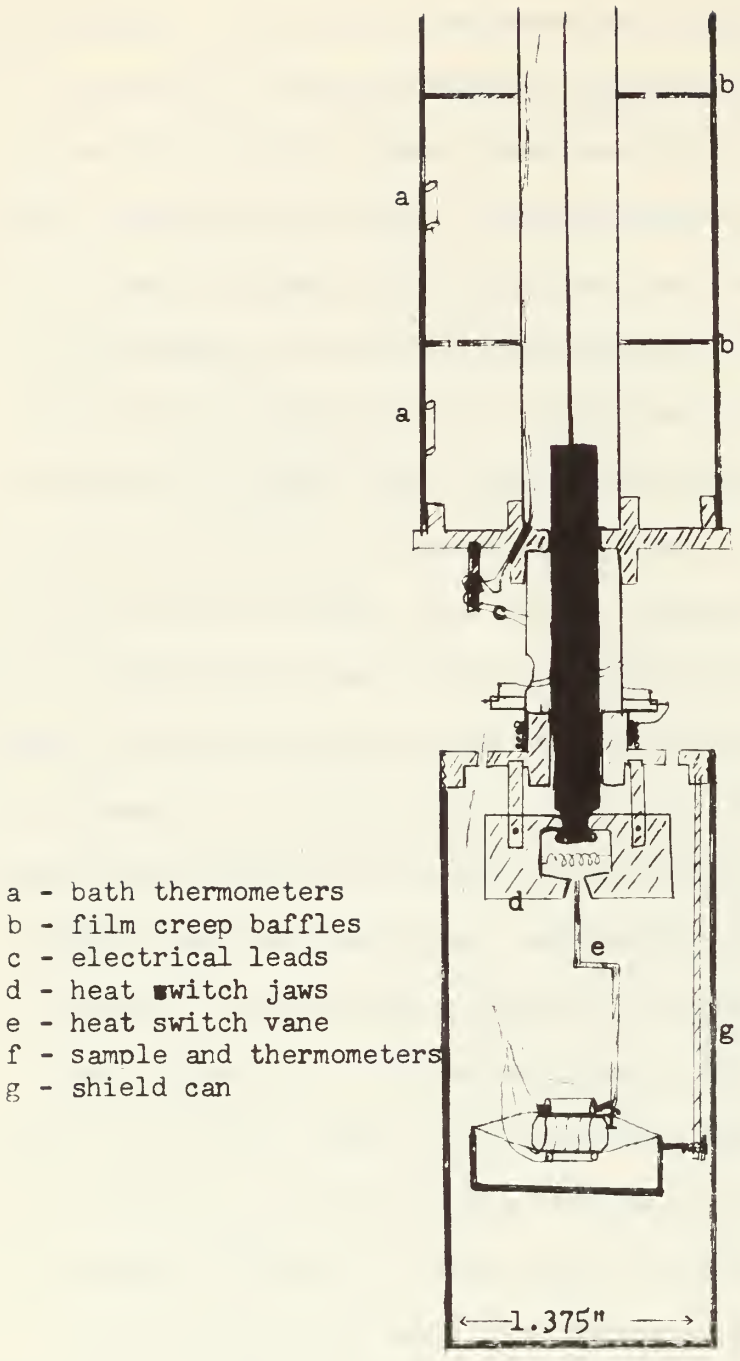

Figure 3: Calorimeter cryostat (lower part)

the top of the can. The bolts are tightened to about 24 inch-pounds of torque to produce a leak-tight joint.

The cryostat top contains electrical outlets for the 22 leads to the shield terminal circle, for the inner bath thermometers, and for the magnet. At the top of the cryostat is a knob which is used to control the heat switch. The needle-valve shaft can be pulled out of the outer helium bath when not in use.

The outer helium bath is contained in a dewar which is surrounded by a jacket filled with liquid nitrogen. Helium is transferred from a storage vessel into the dewar; about six liters is required for the first transfer. This will last for about one day, and successive fillings last for about two days. After transferring, the needle valve is closed, the inner bath pumped to the desired starting temperature, and the heat switch closed. When the sample reaches equilibrium the heat switch is slowly opened. Some heating is produced as the jaws are separated, but the sample returns to equilibrium in about fifteen minutes. At this point the data accural procedure begins as described in part D.

B. TEMPERATURE MEASUREMENT

The temperature of the sample was measured with a carbon resistor (470 ohm, ½ watt, Allen-Bradley Type EB-4). In the region of the specific heat peak (5.3 K) its resistance was about 10,000 ohms and it had a sensitivity of 2×10^{-4} K/ohm. The resistance was measured using a three-lead Wheatstone bridge, operating at 37 Hertz. A lock-in amplifier was used to detect

the null. The power dissipated in the resistor was less than 10^{-8} watts and no heating of the sample by the resistor was detectable at this power. When the largest possible temperature resolution was desired, near the peak, the lock-in amplifier was operated at maximum sensitivity with a time constant of 30 seconds. This allowed resistance changes of 5 parts in 10^7 to be detected, corresponding to a temperature change of 1 microdegree.

The carbon resistor was calibrated by successively recording its resistance and that of the germanium resistor at about 20 equilibrium points over the temperature range 4.2 K - 6 K. The germanium resistor had been previously calibrated as described in Appendix A. The carbon resistor values and corresponding temperatures were fitted to the equation

$$\frac{\log R}{T} = \sum_{i=1}^{6} A_i (\log R)^{i-1}$$

The deviations between the values of T calculated from this formula and the corresponding calibration data points were less than 10^{-3} degrees.

In a magnetic field the resistance of the carbon thermometer increases. This magnetoresistance must be subtracted before entering R in the above equation. This correction was evaluated at 4.2 K by admitting exchange gas into the calorimeter and measuring the resistance as a function of field at fixed temperature. The increase in resistance from the zero field value, ΔR, was found to be related to H by the equation

$$\frac{\Delta R}{R_{|H=0}} = 1.59 \times 10^{-5} H^2 \quad (H \text{ in kilo-oersteds}).$$

There is also a temperature dependence of the magnetoresistance, which has been found to be proportional to $T^{-1.5}$ for Allen-Bradley resistors (Clement 52) (Belanger 69). This temperature dependence was assumed for the thermometers used in this experiment, so that ΔR was calculated from

$$\frac{\Delta R}{R_{|H=0}} = \frac{1.59 \times 10^{-5} (4.22)^{1.5} H^2}{T^{1.5}} .$$

Since $R_{|H=0}$ and T are not known unless ΔR is known, iterations were used: First assuming $R_{|H=0} = R_{|H}$, an approximate ΔR was found, then $R_{|H}$ was corrected and ΔR recalculated. When H = 20 kilo-oersteds, this yields about a .4% correction to R, so that even if ΔR were to be in error by 10%, the corresponding error in T would be about .1 mK. Therefore the error in the temperature scale for all fields used in this experiment is considered to be not more than .5%, as discussed in Appendix A.

C. SAMPLE PREPARATION

Single crystals of $NiCl_2 \cdot 6H_2O$ were grown by slow evaporation of an aqueous solution whose temperature was regulated at 30 °C. The solution was prepared from reagent grade salt supplied by Fisher Scientific Company. Their analysis showed the salt had a cobalt impurity of .03%.

The largest crystal which was used in this experiment had a mass of .76 grams when taken from the growing solution. Its habit is shown in Fig. 4. The angles between the faces were measured and comparison of these angles with published values

(Groth 06) allowed identification of the faces. After the faces were identified, a slice was cleaved parallel to the c face so that this face could be easily identified in the field alignment procedure. The crystal cleaves perfectly along this face since it is the a-b plane in which the layers are formed. This perfect cleavage provided a separate check on the identification of the faces.

The crystal deteriorates badly when exposed to the atmosphere. It is very deliquiscent; that is, it absorbs water from the air, and a layer of solution forms over the crystal. This difficulty was partially overcome by spraying the crystal with a coat of Krylon varnish and dipping it in G.E. 7031 varnish. However, despite these precautions the crystal steadily lost mass; during the experiment its mass was .72 grams. Also the crystal looses water of hydration when placed in a vacuum at room temperature, so that before pumping on the sample, it was first cooled below -30 ^{o}C. After coating the crystal with varnish, a 100 ohm heater made of .002 inch manganin wire was wound tightly around the sample. The heater and sample were then coated again with varnish and allowed to dry for one day. Then germanium and carbon resistance thermometers were mounted on the crystal with nylon thread. A copper wire soldered to one end of the carbon resistor served as the vane to make contact with the heat switch jaws. This assembly was then suspended in a C-shaped sample holder with nylon thread. The sample holder was attached to the shield lid as shown in Fig. 3.

In order to align the easy axis along the vertical magnetic field the sample holder was rotated about the horizontal axis through the center of the sample (the b crystal axis). The correct orientation was determined by making use of the fact that when the c face is inclined 7^{o} from vertical, the easy axis, a", is vertical. This is shown in Fig. 4. A small plastic right triangle with a 7^{o} angle was made, and its hypotenuse was placed against the large cleaved face. The crystal was then rotated until the adjacent side was vertical, as judged by alignment with a vertical rod. It is estimated this procedure was accurate to about $\pm 2^{o}$, which is more precise than the knowledge of the easy axis direction.

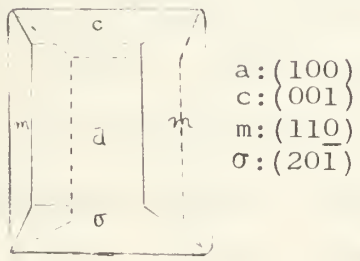

a:(100)
c:(001)
m:(110)
σ:(201)

(a)

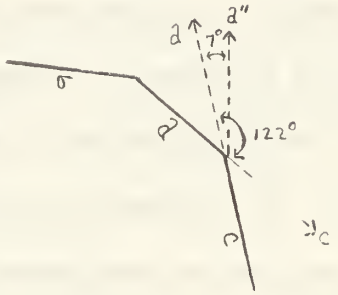

(b)

Fig. 4. (a) Habit of $NiCl_2 \cdot 6H_2O$
(b) Direction of easy axis, a"

D. DATA ACCRUAL

The specific heat measurements begin with the sample in equilibrium with its surroundings, that is, with no detectable drift in its temperature over several minutes. Heat is applied for about 100 seconds; after the heat is turned off the sample and thermometer quickly achieve equilibrium. Unless the shield temperature is adjusted to be equal to the new sample temperature, a slow cooling of the sample will be observed at the end of the heating period. To prevent this non-adiabatic condition, a guess is made of the sample temperature change during the heating period; half-way through the heating, the shield temperature is set to match the estimated final sample temperature. In this way the shield is colder than the sample for the first half of the period and warmer for the last half. The adjustment of the shield is made easy because similar resistors are used for shield and sample thermometers, so that the resistance change during a heating period is about the same for both. If this procedure is followed carefully, adiabatic conditions can be maintained during the measurements, and after the heat is turned off, the sample temperature remains perfectly constant. After a series of several heating steps are made, the sample temperature is monitored for more than 15 minutes; any slight drift in temperature is compensated by small adjustments of the shield temperature.

The power to the heater is provided by a voltage divider across a 1.35 volt mercury cell. Four leads go to the heater, two carry the current and two are used to measure the potential

across the heater. In series with the current lead is a 100 ohm standard resistor, so that both V and I can be measured with a potentiometer which is read to $\pm 10^{-6}$ volts (Leeds and Northrup, Model K-3). The heating period is timed with a digital clock (Anadex Model CF200) accurate to $\pm$ .01 seconds. The source of power for the sample heater was stable enough so that the power usually remained constant through out the heating period. Heating steps were about 1 millidegree and the applied power was as small as .1 microwatt near the specific heat maximum.

Errors in a measurement of the heat capacity can arise from uncertainties in the power, time, and temperature rise. The measured valued of power and time are considered accurate to .01%. Stray heating or cooling occurs whenever the shield and sample temperatures are not equal. As explained above, the shield was adjusted in only a few increments during the heating, but the cooling and heating effects should cancel. When large temperature steps were taken the uncertainty in the adiabaticity of the measurement increased, but the errors were random. Errors in the temperature rise can occur when there is drift after a heating period. If there was drift, the resistance was extrapolated back to the expected equilibrium time (about five seconds after the power was turned off). If the drift was excessive, a notation was made; and, if the corresponding specific heat point seemed in error from an examination of a graph of the data, that point was discarded (ten points were discarded for this reason). An error in calculation of the temperature rise can be made when the fitting formula for T vs R is used to convert ΔR to ΔT. This

uncertainty is difficult to evaluate, but from experience gained in measurements of the heat capacity of metals it is felt this error is negligible. When calculating the specific heat from the measured heat capacity uncertainties in the mass of the sample add to the total uncertainty. In this experiment the mass is quite imprecise. For the large crystal the mass was evaluated as .72 $\pm$ .01 grams. Thus the absolute value of the specific heat data has an uncertainty of $\pm$ 2%. The major uncertainty in the heat capacity comes from determining the temperature change. Due to uncertainties in this factor, the precision of the heat capacity is estimated as approximately .3% near the peak and .8% away from the peak.

V. RESULTS AND CONCLUSIONS

A. INTRODUCTION

Three experiments were done using different samples of $NiCl_2 \cdot 6H_2O$. The first measurements were made on a small crystal furnished by R.L. Kleinberg. Data in zero field and in several applied fields were taken. At the end of this first experiment, several factors indicated the desirability of a second experiment. A larger single crystal had been grown, which would allow more accurate alignment of the easy axis with the field and more precise heat capacity measurements. Also significant improvements were made in the sensitivity of the sample thermometer bridge, and a stray source of heat input to the sample was eliminated.

The second experiment was carried out on a .72 gram single crystal in zero field. Preliminary analysis of the data showed that the heat capacity peak was broader and occured at a slightly lower temperature than that of the smaller crystal. To verify that this effect was reproducible and was caused by differences in the crystals, it was decided to replace this large crystal with another of Dr. Kleinberg's small crystals.

The third experiment used a sample with a mass of about .1 grams. Applied fields of approximately 1, 5, 10, and 20 kilooersteds were used. This set of data essentially duplicated that of the first experiment, and it was of higher quality, therefore no further analysis was carried out on the first set of data.

In the following discussion the set of data from the second experiment is referred to as the "large crystal data", and that from experiment three is the "small crystal data".

In this section the magnetic contribution to the specific heat of these two samples is analyzed and compared with predictions made by theoretical models.

B. ADDENDA AND LATTICE CORRECTIONS

To determine the magnetic specific heat, it is necessary to evaluate the contributions to the measured heat capacity from the lattice and from the attachments to the sample. In this experiment the addenda consisted of: germanium and carbon resistors, manganin heater wire, nylon threads, a copper heat-switch vane, and varnish. Since the heat capacity of this assembly was quite small, it was decided that a calculation of the addenda contribution would be as accurate as a measurement of it. Each component of the addenda was weighed separately (except the varnish) and the entire sample and addenda were weighed before and after an experiment. From published data, formulas were developed which approximated the heat capacity of each part of the addenda as a function of temperature. The values calculated from each formula, evaluated at the temperature of each data point, were added, and the total subtracted from the measured heat capacity. The addenda contribution comprised about 1% of the total heat capacity at the lowest temperature reached, 2% at the highest temperatures, and .3% at the heat capacity peak.

The lattice heat capacity is expected to vary as T^3 in the temperature range covered in this experiment, since the Debye temperature of the salt is about 200 K. The lattice background had been separated from the total specific heat previously (Robinson 60). According to this separation,

$$C_L = (1.503 \times 10^{-3})\ T^3 \text{ joules/mole-degree.}$$

This expression was used to evaluate the lattice contribution. This contribution varied from 1% at 4.3 K to 5% at 5.8 K, and was .6% of the total at the heat capacity peak.

To find the molar specific heat, C_p, the measured heat capacity was divided by the number of moles. The mass of the large crystal was known to about 1.5%, however the mass of the smaller crystal was more uncertain. Because the mass of the varnish was not as well established, a large uncertainty existed in the heat capacity of the addenda for experiment three. For these reasons, the small crystal results were normalized to match the large crystal's specific heat at the lowest and highest temperatures. This is justified because at temperatures far away from the peak, both heat capacity curves had the same shape.

C. RESULTS IN ZERO APPLIED FIELD

Application of the corrections described in Part B yielded the magnetic specific heat, C_m, for the large and small crystals. The results for zero field are given in Tables II and III and plotted in Figs. 5 and 6. Each point is shown on these graphs, except the ten points which were rejected because of excessive drift.

The data show the familiar lambda-shaped peak which is characteristic of magnetic and other cooperative phase transitions. However, closer inspection of the temperature region near the peak shows that the specific heat is rounded (Fig. 7). The small sample shows a sharper peak, and its specific heat at the peak is 12% greater than that of the large sample. The temperatures at which maxima occur differ for the two crystals: T_{max} is 5.335 K for the large crystal and 5.338 K for the small one. This shift is larger than possible shifts in the temperature scale between experiments.

The functional form of the data in zero field is of interest for comparison with theoretical predictions. The rounded peak makes such a determination less than straight-forward. The first difficulty is the location of the "transition temperature", T_N. As a first approximation this might be taken to be the temperature at which the heat capacity maximum occurs, T_{max}. However here, and in most experiments, T_N is treated as a parameter and allowed to wander somewhat from the maximum if a considerably better fit results. Although T_N is treated as a fitting parameter, it is considered as having physical significance: if the sample were an infinite perfect array, then T_{max} should equal T_N.

It is useful to specify three temperature regions for the data. First, some points are too far from the peak to be considered as critical data; some points near the maxima are not considered critical data because of the rounding; and finally there are data on each side of the peak which are considered truly representative of ideal sample behavior. It is this last

region on which attention is focused. The boundaries between these regions are somewhat hazy, and the ultimate results may depend somewhat on the choice of data used in the analysis. This dependence can be checked by observing the effect of a movement of the boundaries used for data analysis on the results. For the analysis presented here, it was found that the determination of critical parameters was not very sensitive to the readjustment of boundaries, and a visual determination of the rounded region and the extreme regions from graphs was sufficient.

The analysis of the functional form of C vs T began with inspection of semilogarithmic plots, C vs log $(1 - T/T_{max})$ (Fig. 8). The points, $T < T_{max}$, seem to lie roughly on a straight line, however, for $T > T_{max}$ the points definitely do not fall on a straight line. Next, log C was plotted against log $(1 - T/T_{max})$. On this graph, the high temperature points fall more nearly on a straight line; however, a single straight line does not fit these points well.

The next step of the data analysis was to fit C to the functional form suggested by theory, Equations II-4:

$$C_+ = A/\alpha[\epsilon^{-\alpha} - 1] + B \quad \text{for } T > T_N$$

$$C_- = A'/\alpha'[\epsilon^{-\alpha'} - 1] + B' \quad \text{for } T < T_N.$$

(For α or $\alpha' = 0$, a logarithmic fit was used.) The procedure adopted was that suggested by van der Hoeven (68). The analysis for temperatures above T_N is explained below; the same procedure was followed for $T < T_N$. Values of α and T_N (in this case called

T_{N+}) are chosen. A and B are then determined by a linear least squares fit of that portion of the data which are chosen to represent the "ideal" region above T_{N+}. Using the values of A and B, the difference between the measured and calculated values of C are found, and the correlation coefficient[1] for this fit is found. Next T_{N+} is changed by .2 mK and the procedure is repeated. This process is repeated until all reasonable values of T_N have been tested. (T_N was allowed to range from 5.335 K to 5.350 K.) This entire procedure is then repeated for different values of α. After the process is completed, one has a family of curves corresponding to different values of α. An example of such a family is shown in Fig. 9. Each curve shows the correlation coefficient as a function of T_{N+} for fixed α. Each curve has a maximum, and there is a largest maximum. The values of α and T_{N+} which produce the largest correlation coefficient are chosen as the best representation of the data; corresponding to this choice are constants A and B which give the fit of the equation to the data. In applying this procedure to data below T_N, another set of parameters, α', T_{N-}, A', and B' are found. Since T_N was allowed to vary over such a large range, the data set being fitted was modified for each assumed T_N so that no points fell within 3 mK of T_N. The analysis procedure was tested many times using different choices for the regions

---

[1]The correlation coefficient, γ, is defined by $\gamma = \sqrt{1-\delta/N\sigma^2}$, where δ is the sum of the square deviations, N the number of points used, and σ^2 the variance of the data. γ is a measure of how well a set of points is correlated to a functional fit. Its value is one if the fit is perfect.

over which the data were fit and the criterion used for the rejection of data as being too near T_N. The fitting parameters were relatively insensitive to the choices. Thus, it is felt that a meaningful fit to the data was achieved. An estimate of the uncertainty in the fitting parameters can be made by determining the range over which a parameter can vary from its best value before the points systematically deviate from the function. The results of this procedure are summarized below:

	Small Crystal	Large Crystal
T_{N+}	5.348 ± .001 K	5.348 ± .001 K
α	.20 ± .03	.17 ± .03
A	.835	.866
B	3.9	3.9
γ	.997	.998
	---	---
T_{N-}	5.3476 ± .001 K	5.3466 ± .001 K
α'	.00 ± .01	.00 ± .03
A'	5.15	4.6
B'	1.858	2.2
γ	.9999	.9995

It can definitely be said that the data for both crystals below T_N can be fit best with a logarithm. Above T_N a power law is best. The best value of T_N seems to be about .01 K higher than T_{max}. It is not possible to say that this temperature has physical significance; but, since both samples

have about the same T_N, it appears that it is more than an artifact of the fitting procedure. This type of behavior has been found to hold in many magnetic transitions. For example, In $MnCl_2 \cdot 4H_2O$, where rounding was less of a problem, $\alpha = .35$ and $\alpha' = 0$ (Dixon 69); in MnF_2, $0 \leq \alpha < 1$ and $\alpha' = 0$ (Teaney 65).

As a measure of width of the peak, the interval Δ is defined to be the temperature between specific heat points which are 90% of the maximum. These values are given in Table I. The width for the small crystal is .014 K and for the large crystal, .021 K. Also the maximum heat capacity is less for the large crystal. These observations are qualitatively in agreement with theoretical arguments given in Section II. If the values of T_N described above are valid, then the theoretical prediction that the shift in the maximum from T_N is related to the size of imperfections can be applied. Using equations II-5 and $T_N - T_{max} = .01$ K, one obtains the estimate of 500 atoms between boundaries.

The next step in the analysis of the data was to introduce another fitting parameter, τ, to fit the data using the temperature variable, ϵ^*, of equation II-6. All data in the rounded region were included and the points below T_{max} were fitted to

$$C_- = A'/\alpha'(\epsilon^{*-\alpha'} - 1) + B',$$

where

$$\epsilon^* = \left\{ \left(\frac{T - T_{max}}{T_N} \right)^2 + \left(\frac{\tau}{T_N} \right)^2 \right\}^{\frac{1}{2}}.$$

T_{max} and T_N had already been determined so that α' and τ were allowed to vary, and the pair that produced the best fit were determined as described above. The following values were obtained as the best values of the fitting parameters:

	Large Crystal ($T_N - T_{max} = 11$ mK)	Small Crystal ($T_N - T_{max} = 9$ mK)
τ	10 mK	5 mK
α'	0.0	0.0
A'	4.14	3.91
B'	3.6	6.07
γ	.9993	.998

Figure 11 shows the large crystal data with a curve representing the fitting equation using the best value of α', τ, A' and B'. Also shown is an undamped logarithmic singularity corresponding to $\tau = 0$. The significant feature of these results is that in both cases τ is approximately equal to $T_N - T_{max}$, as predicted theoretically (Fisher 67) for two-dimensional Ising arrays (the width may be less than the shift for three-dimensional lattices). The procedure was also applied to data above T_N, but it did not converge to a unique value of τ and α.

One can speculate concerning the differences in the large and small crystals. They originated from different laboratories, and no information is available on the impurity level of the small crystal; however, it is probably about the same as for the large one, both having been grown from commercial reagent-grade chemicals. Outwardly the small crystal appeared less

perfect than the large crystal, but it is likely that the smaller one had fewer strains and imperfections. The fact that the size and impurity level of a sample can change its transition temperature has been previously observed. The heat capacity of two high-quality single crystals of MnF_2 have been measured (Teaney 65), one with a mass three times the other. The transition temperature of the larger crystal was .1 K lower than that of the small one ($T_N \approx 67.3$ K). The effect of impurities on the phase transition in Gd has been studied (Cadieu 68); it was found that impurities reduce the transition temperature.

D. RESULTS IN APPLIED FIELDS

Data obtained for various magnetic fields along the easy axis are given in Tables IV through VII and plotted in Fig. 12. Fig. 12 shows all of the applied field data on one graph. Two general features are apparent: The heat capacity maxima are shifted to lower temperatures, and they are reduced in magnitude. The shape of the curves does not change significantly away from the peak. Although there is not enough data at all fields to attempt a functional fit, as was done in zero field, the data retain the shape of the zero field curves when plotted on semi-logarithmic graphs.

In order to determine the effect of the field on the rounding of the peak, a width of each peak was measured as described in part C. The width value, Δ, listed in Table I, definitely increases with field; however, no quantitative conclusions were reached about this dependence.

If the view is adopted that T_{max} is not the theoretically discussed T_N, but is shifted from T_N by imperfections or impurities, it follows that the same shift should apply in finite fields, and hence

$$T_{max}(0) - T_{max}(H) = T_N(0) - T_N(H).$$

This allows comparison of this experimental data to the predictions about the phase boundary $T_N(H)$. Both mean field and Ising theories predict that a plot of $[T_N(0)-T_N(H)]/T_N(0)$ against H^2 (for $H \ll H_c$) will yield a straight line. Although the experimental points are sparce, they do seem to fall on a line with slope $9 \times 10^{-11}(Oe)^{-2}$. This agrees only in order of magnitude with the mean field prediction; while the three-dimensional Ising model predicts a slope of $16 \times 10^{-11}(Oe)^{-2}$.

E. CONCLUSIONS

The specific heat of $NiCl_2 \cdot 6H_2O$ has been measured in zero and applied fields. The temperature resolution was sufficient to study the rounding of the peak that occurs over a few millidegrees. The zero field data is seen to be in good agreement with estimates of the critical behavior of theoretical models. It is necessary to use a Néel temperature about 10 millidegrees higher than the temperature at which the specific heat maximum occurs. The best estimate of the Néel temperature is $5.3475 \pm .001$ K.

The concept of a complex transition temperature is used to introduce a fitting parameter to describe the rounding and the shift of the peak. This seems promising and hopefully can be put on firmer theoretical footing. The tentative conclusion is that the basic cause of the non-ideal behavior are crystalline imperfections. These restrict the range of correlations and lower the transition temperature of the small homogeneous regions. The broadening is caused by the distribution of sizes of these regions, each with a separate transition temperature. This conclusion is supported by the observation, using NMR, that both antiferromagnetic and paramagnetic phases coexist over a range of 10^{-2}K about the transition temperature in $CoCl_2 \cdot 6H_2O$ (Sawatzy 64).

The phase boundary between paramagnetic and antiferromagnetic states was determined for fields up to 20 kOe. While the shape is in qualitative agreement with simple theoretical predictions, there is no quantitative agreement. The transition remains fairly sharp in applied fields, although the maxima decrease in magnitude and the rounding is slightly increased.

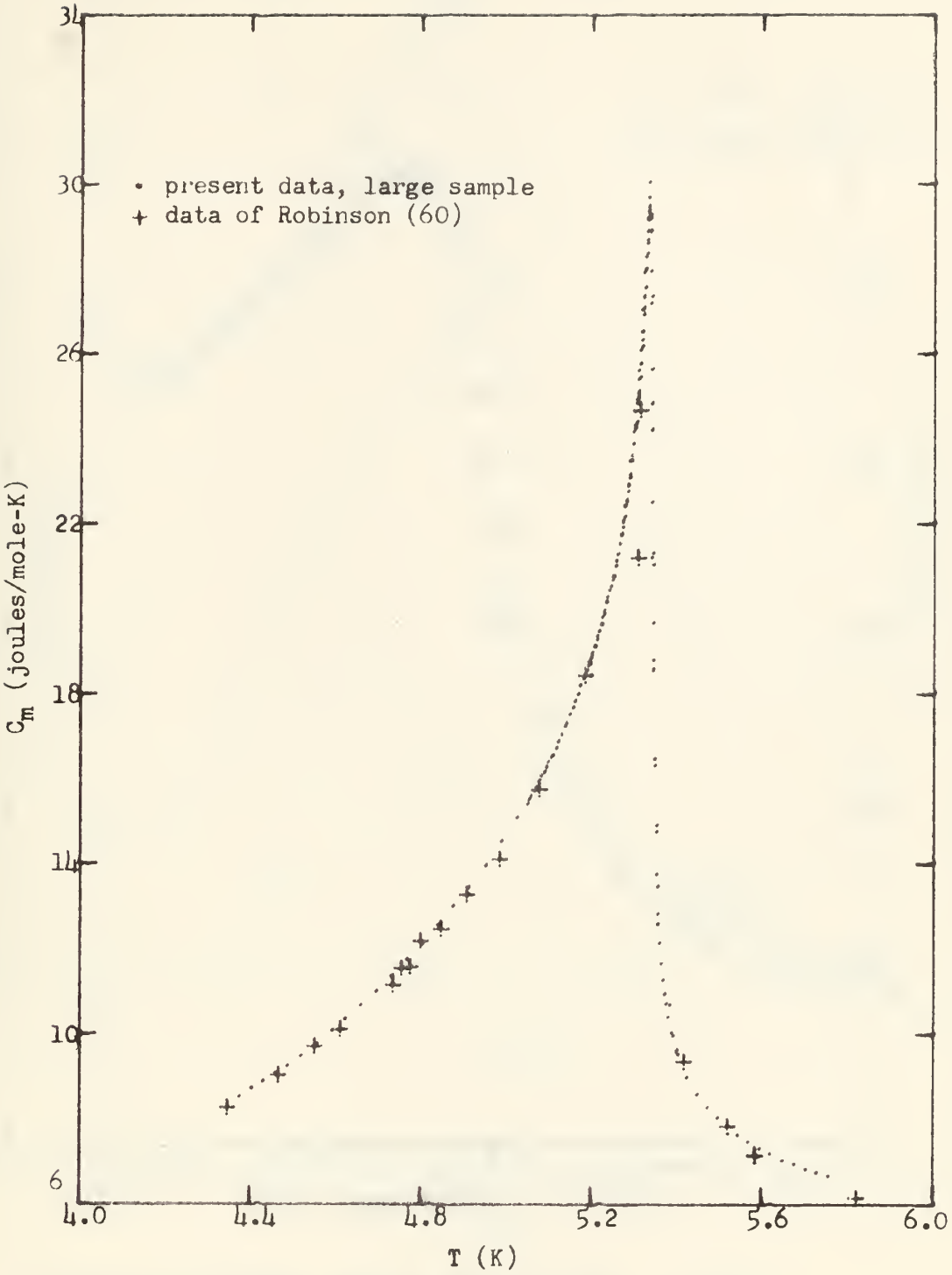

Figure 5: Magnetic specific heat of $NiCl_2 \cdot 6H_2O$

Figure 6: Specific heat of small sample, zero field

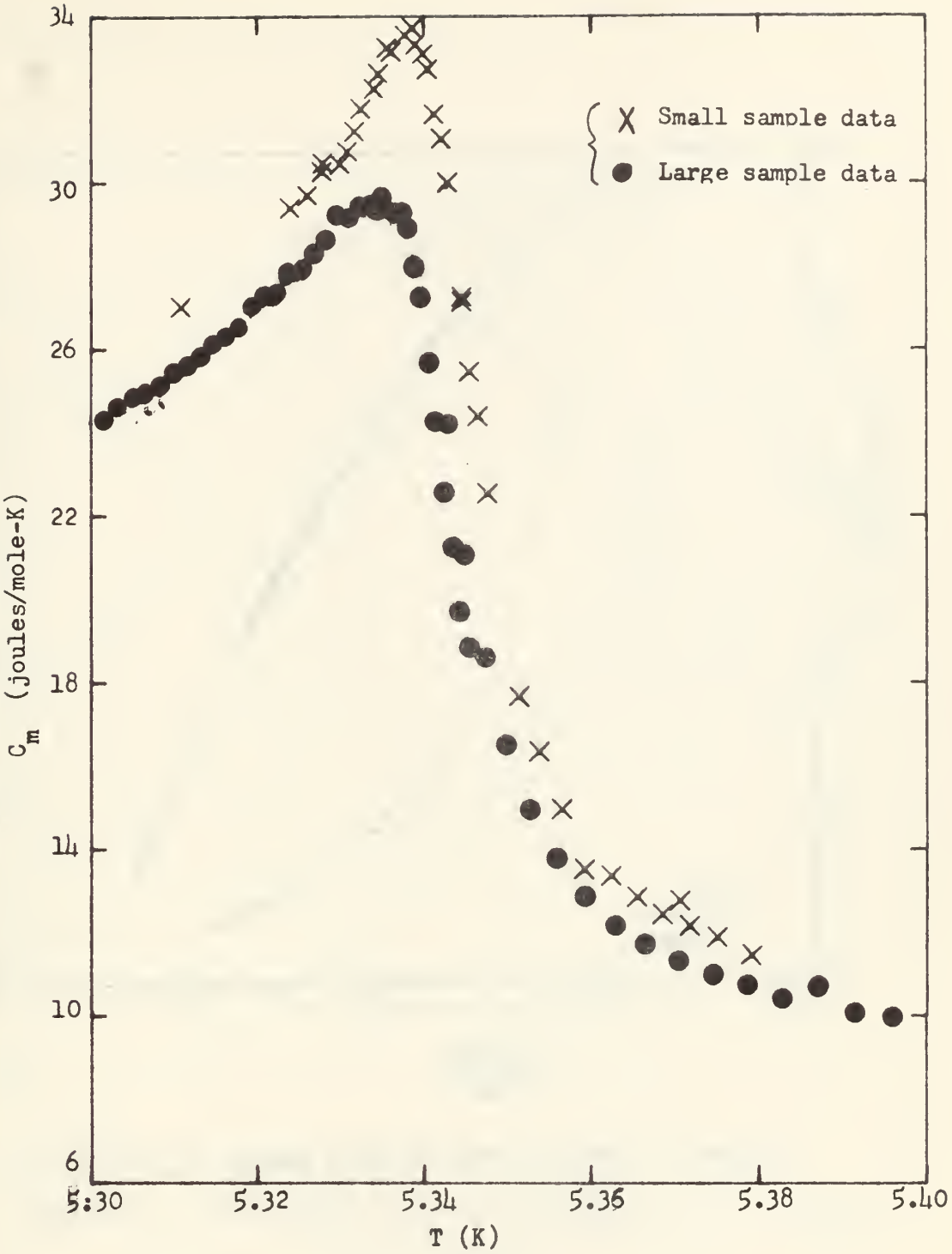

Figure 7: Specific heat of $NiCl_2 \cdot 6H_2O$ in zero field near the Néel temperature[2]

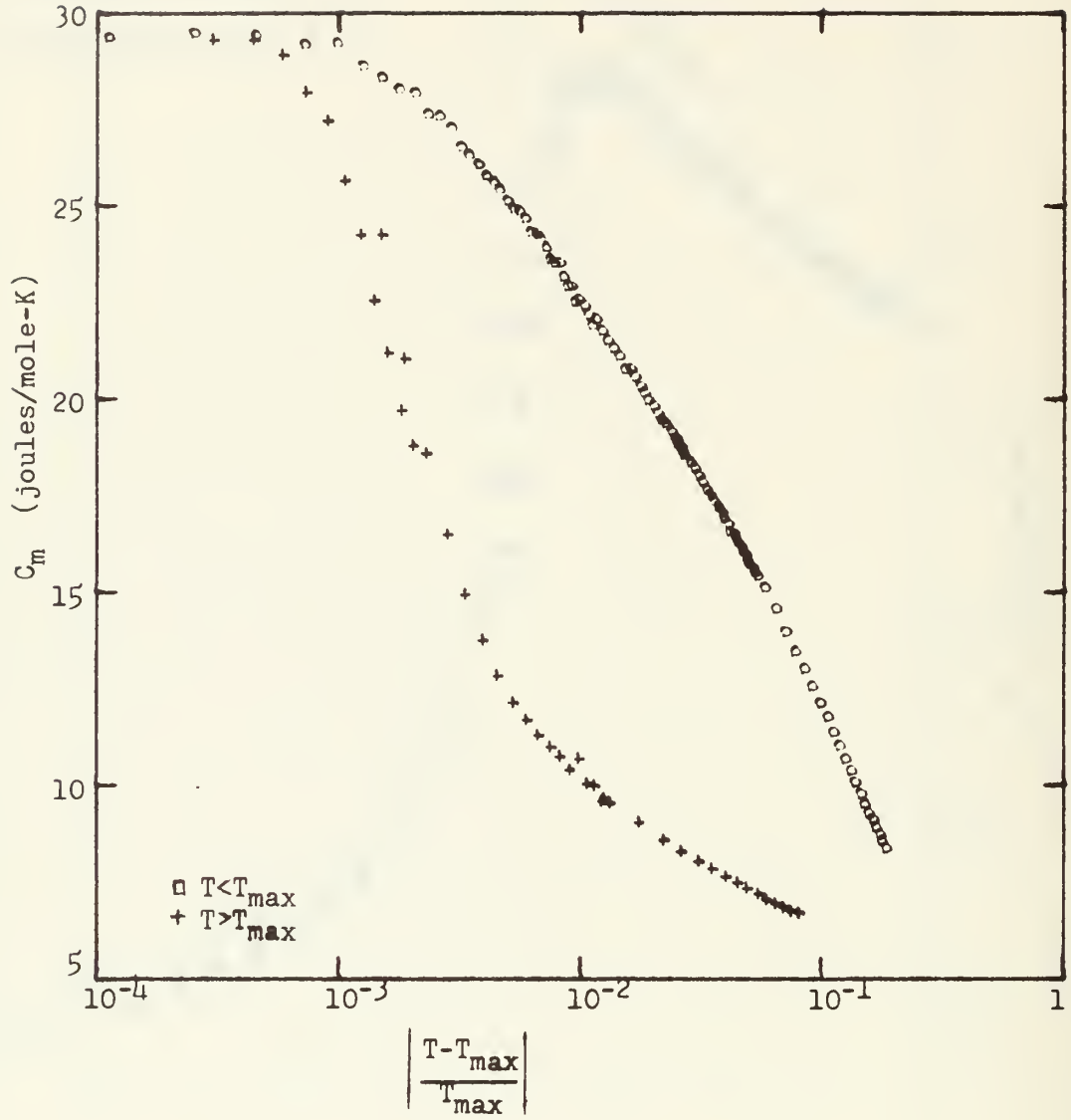

Figure 8: Specific heat of large sample, T_{max}=5.335 K

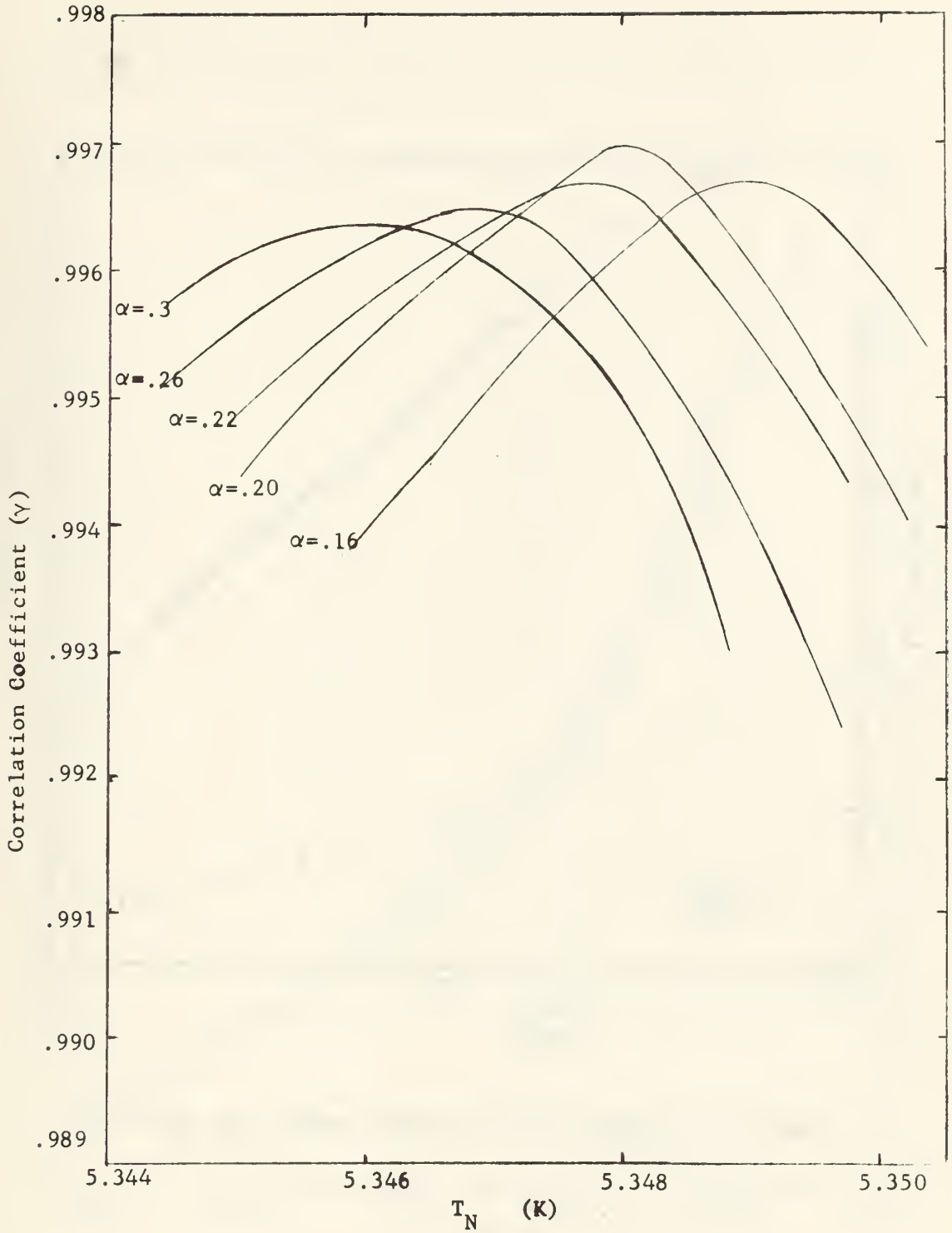

Figure 9: Correlation coefficients for fit of Eq. II-4 to large crystal data ($T>T_N$) using various values of α and T_N.

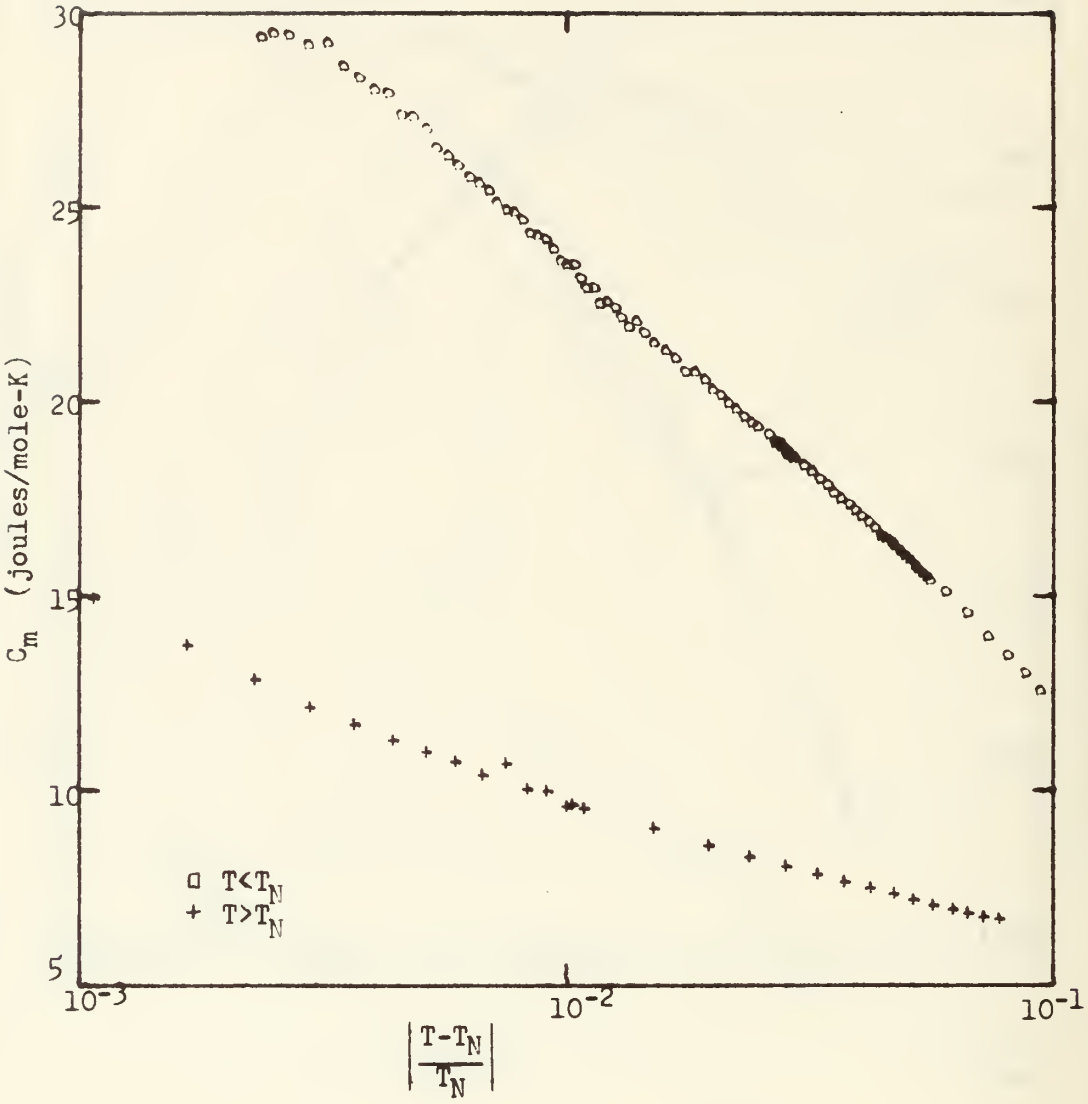

Figure 10: Specific heat of large sample with T_N=5.347

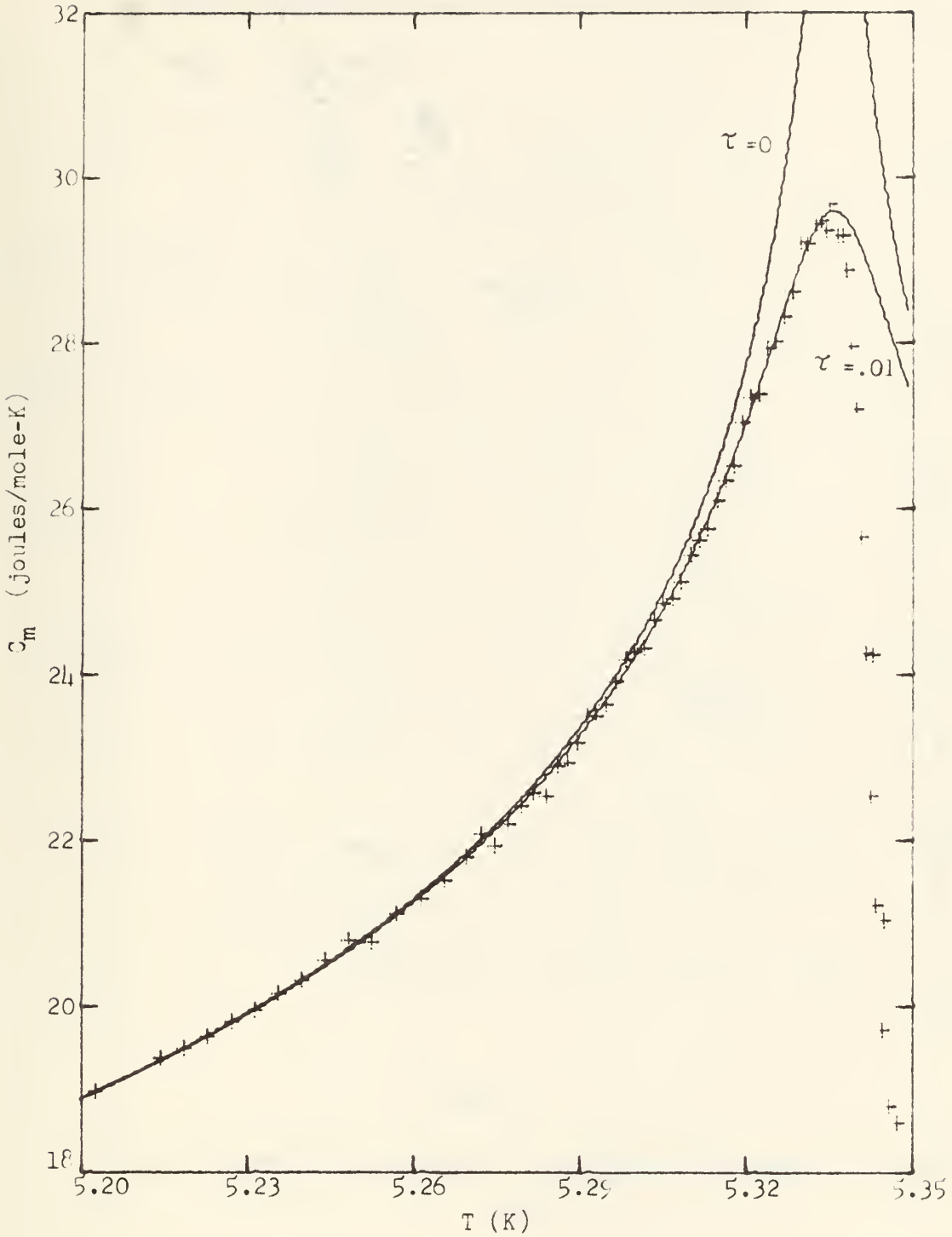

Figure 11: Large sample data with fitted curves

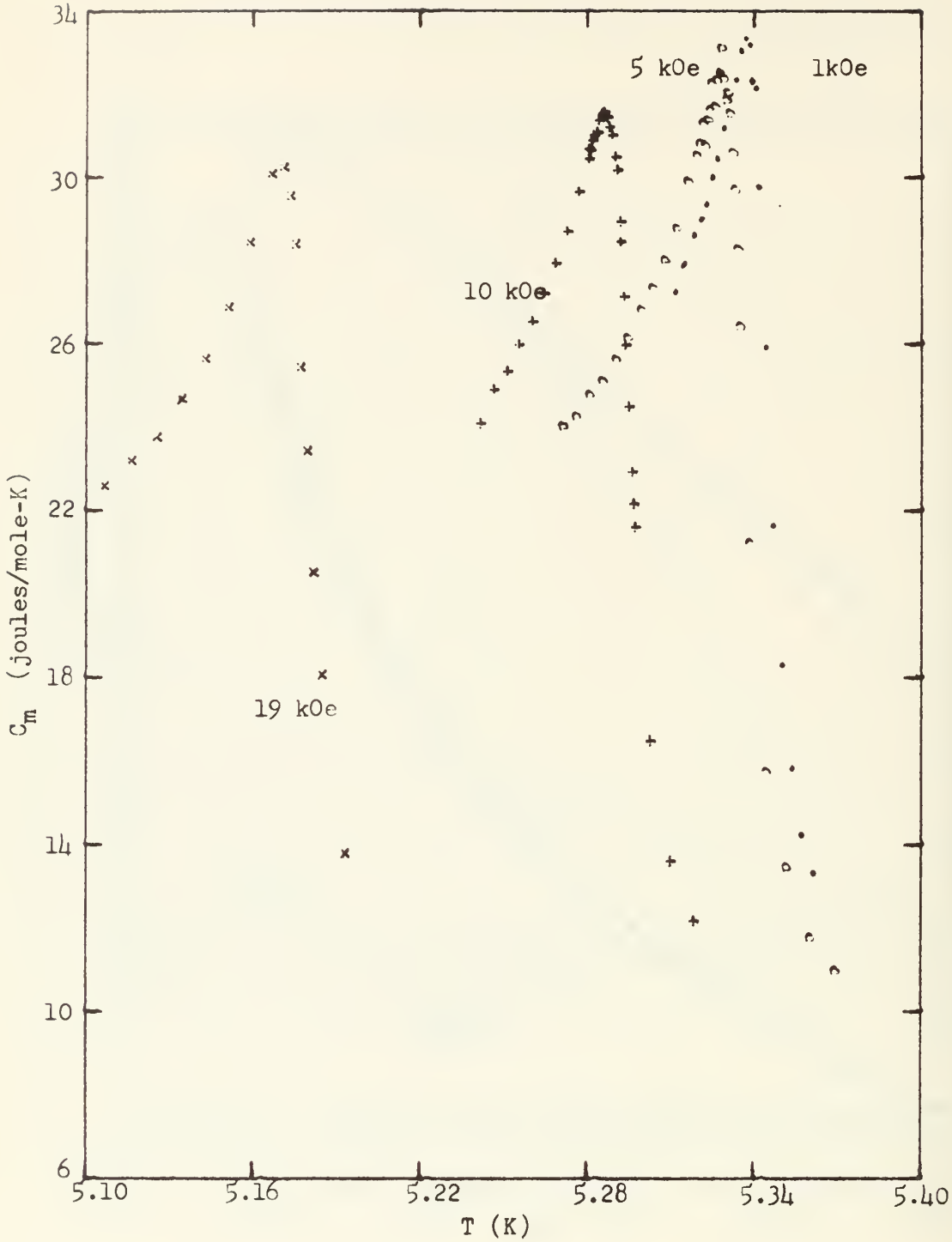

Figure 12: Specific heat of $NiCl_2 \cdot 6H_2O$ in applied fields

	T_{max} (K)	C_{max} (joules/mole-K)	Δ (K)
Large Crystal			
H = 0	5.335	29.6	.021
Small Crystal			
H = 0	5.338	33.6	.014
H = 1	5.337	33.4	.016
H = 5	5.327	33.1	.018
H = 10	5.286	31.6	.020
H = 19	5.170	30.4	.022

T_{max}: temperature at which C_m is largest

C_{max}: largest value of C_m

Δ : temperature interval for $C = .9C_{max}$

TABLE I

Tables II - VII give the magnetic contribution to the specific heat, C_m, of $NiCl_2 \cdot 6H_2O$ in various fields.

T is the average of the initial and final temperatures of a heating step.

C_m is the molar magnetic specific heat. Its units are joules/mole-K. The total specific heat, C_p, may be found by $C_p = C_m + 1.503 \times 10^{-3} T^3$.

Delta T is the difference between the final and initial temperature (the size of the heating step).

TABLE II LARGE SAMPLE H = 0 K OE

	T	CM	DELTA T
1	4.3502	8.3966	0.0293
2	4.3792	8.5508	0.0288
3	4.4076	8.7355	0.0281
4	4.4355	8.9153	0.0276
5	4.4628	9.1032	0.0270
6	4.4895	9.2713	0.0266
7	4.5207	9.5034	0.0358
8	4.5568	9.7796	0.0365
9	4.5927	10.0839	0.0354
10	4.6279	10.3887	0.0353
11	4.6623	10.6875	0.0336
12	4.6983	11.0257	0.0384
13	4.7353	11.3986	0.0357
14	4.7707	11.7639	0.0352
15	4.8070	12.1399	0.0374
16	4.8427	12.5791	0.0340
17	4.8779	13.0011	0.0366
18	4.9153	13.4673	0.0382
19	4.9541	13.9985	0.0394
20	4.9914	14.5517	0.0351
21	5.0270	15.1077	0.0361
22	5.0482	15.4318	0.0059
23	5.0541	15.5277	0.0058
24	5.0599	15.6213	0.0058
25	5.0657	15.7431	0.0058
26	5.0715	15.8334	0.0057
27	5.0772	15.9724	0.0057
28	5.0828	16.0814	0.0056
29	5.0884	16.1781	0.0056
30	5.0940	16.3135	0.0056
31	5.0996	16.4084	0.0055
32	5.1051	16.5452	0.0055
33	5.1106	16.5883	0.0055
34	5.1167	16.7594	0.0068

TABLE II LARGE SAMPLE H = 0 K OE

	T	CM	DELTA T
35	5.1235	16.9006	0.0068
36	5.1303	17.0537	0.0067
37	5.1369	17.2404	0.0066
38	5.1436	17.3553	0.0066
39	5.1501	17.5243	0.0066
40	5.1567	17.6874	0.0065
41	5.1632	17.8700	0.0064
42	5.1696	18.0367	0.0064
43	5.1759	18.2130	0.0063
44	5.1822	18.3919	0.0063
45	5.1885	18.5817	0.0062
46	5.1912	18.5738	0.0022
47	5.1945	18.6835	0.0044
48	5.1946	18.7632	0.0061
49	5.1964	18.7277	0.0062
50	5.1988	18.8653	0.0043
51	5.2008	18.9724	0.0061
52	5.2026	18.9006	0.0063
53	5.2028	18.9889	0.0035
54	5.2068	19.1593	0.0060
55	5.2091	19.1472	0.0066
56	5.2144	19.3709	0.0042
57	5.2152	19.2809	0.0057
58	5.2186	19.4929	0.0043
59	5.2229	19.6465	0.0043
60	5.2253	19.6683	0.0046
61	5.2272	19.8282	0.0043
62	5.2309	19.8910	0.0066
63	5.2315	19.9604	0.0043
64	5.2358	20.1662	0.0042
65	5.2372	20.1659	0.0060
66	5.2399	20.3119	0.0041
67	5.2434	20.4410	0.0066
68	5.2441	20.5525	0.0043

TABLE II LARGE SAMPLE H = 0 K OE

	T	CM	DELTA T
69	5.2483	20.7929	0.0042
70	5.2500	20.7188	0.0066
71	5.2526	20.7736	0.0044
72	5.2569	21.0377	0.0070
73	5.2570	21.1269	0.0044
74	5.2614	21.3049	0.0044
75	5.2658	21.5272	0.0044
76	5.2695	21.7962	0.0031
77	5.2696	21.7484	0.0053
78	5.2722	22.0894	0.0021
79	5.2745	22.0464	0.0052
80	5.2746	21.9421	0.0028
81	5.2772	22.1917	0.0023
82	5.2795	22.4138	0.0022
83	5.2797	22.4569	0.0051
84	5.2817	22.5882	0.0023
85	5.2840	22.5497	0.0023
86	5.2846	22.7707	0.0046
87	5.2860	22.9056	0.0018
88	5.2878	22.9406	0.0018
89	5.2893	23.1158	0.0048
90	5.2896	23.1843	0.0018
91	5.2914	23.5099	0.0017
92	5.2931	23.5098	0.0017
93	5.2940	23.5179	0.0046
94	5.2949	23.6307	0.0017
95	5.2966	23.9193	0.0017
96	5.2983	24.1778	0.0017
97	5.2985	23.8875	0.0045
98	5.3000	24.2785	0.0017
99	5.3017	24.3190	0.0017
100	5.3030	24.3318	0.0044
101	5.3034	24.6648	0.0017
102	5.3051	24.8665	0.0017

TABLE II LARGE SAMPLE H = 0 K OE

	T	CM	DELTA T
103	5.3062	24.4102	0.0021
104	5.3067	24.9260	0.0016
105	5.3083	24.9940	0.0021
106	5.3084	25.1240	0.0016
107	5.3100	25.4400	0.0016
108	5.3105	25.0700	0.0023
109	5.3116	25.6285	0.0016
110	5.3128	25.4497	0.0023
111	5.3132	25.7617	0.0016
112	5.3148	26.0934	0.0016
113	5.3151	25.7820	0.0022
114	5.3164	26.3420	0.0016
115	5.3173	26.1960	0.0022
116	5.3179	26.5266	0.0015
117	5.3193	26.5339	0.0019
118	5.3194	27.0493	0.0015
119	5.3210	27.3460	0.0015
120	5.3211	26.9515	0.0018
121	5.3225	27.3832	0.0015
122	5.3230	27.1056	0.0018
123	5.3239	27.9448	0.0015
124	5.3248	27.5738	0.0018
125	5.3254	28.0113	0.0015
126	5.3265	28.0198	0.0018
127	5.3269	28.3144	0.0015
128	5.3283	28.3747	0.0017
129	5.3283	28.6273	0.0014
130	5.3298	29.2107	0.0014
131	5.3300	28.6957	0.0017
132	5.3312	29.1919	0.0014
133	5.3317	28.9045	0.0017
134	5.3326	29.4411	0.0014
135	5.3334	29.3693	0.0017
136	5.3336	29.4878	0.0008

TABLE II LARGE SAMPLE H = 0 K OE

	T	CM	DELTA T
137	5.3344	29.3561	0.0007
138	5.3351	29.1876	0.0017
139	5.3351	29.6872	0.0007
140	5.3359	30.0517	0.0007
141	5.3366	29.2940	0.0007
142	5.3368	29.2122	0.0017
143	5.3374	29.2915	0.0007
144	5.3381	28.8840	0.0008
145	5.3385	28.9292	0.0017
146	5.3389	27.9650	0.0008
147	5.3398	27.2007	0.0010
148	5.3403	27.3940	0.0018
149	5.3407	25.6627	0.0009
150	5.3415	24.2574	0.0009
151	5.3422	24.8617	0.0020
152	5.3425	22.5406	0.0010
153	5.3429	24.2318	0.0019
154	5.3435	21.2117	0.0010
155	5.3443	21.3278	0.0023
156	5.3445	19.7123	0.0011
157	5.3450	21.0494	0.0022
158	5.3457	18.8009	0.0012
159	5.3468	18.5889	0.0026
160	5.3473	18.6090	0.0024
161	5.3496	16.3273	0.0030
162	5.3499	16.5155	0.0027
163	5.3527	14.9287	0.0030
164	5.3528	14.7699	0.0033
165	5.3559	13.7629	0.0033
166	5.3562	13.5147	0.0036
167	5.3593	12.8556	0.0035
168	5.3599	12.6267	0.0038
169	5.3628	12.1621	0.0037
170	5.3666	11.6888	0.0038

TABLE II LARGE SAMPLE H = 0 K OE

	T	CM	DELTA T
171	5.3705	11.2886	0.0040
172	5.3746	10.9772	0.0041
173	5.3787	10.7436	0.0042
174	5.3829	10.4235	0.0043
175	5.3871	10.6816	0.0042
176	5.3914	10.0676	0.0044
177	5.3959	9.9931	0.0044
178	5.4004	9.6224	0.0046
179	5.4021	9.6595	0.0249
180	5.4050	9.5587	0.0046
181	5.4277	9.0309	0.0263
182	5.4520	8.6145	0.0223
183	5.4746	8.3199	0.0230
184	5.4980	8.0634	0.0237
185	5.5221	7.8499	0.0243
186	5.5467	7.6523	0.0249
187	5.5717	7.5059	0.0254
188	5.5974	7.3480	0.0259
189	5.6234	7.2107	0.0263
190	5.6498	7.0703	0.0268
191	5.6768	6.9663	0.0271
192	5.7041	6.8642	0.0275
193	5.7318	6.7642	0.0279
194	5.7598	6.6814	0.0282

TABLE III SMALL SAMPLE H = 0 K OE

	T	CM	DELTA T
1	4.3342	8.3291	0.0303
2	4.3633	8.4522	0.0285
3	4.3929	8.7186	0.0304
4	4.4248	8.9496	0.0338
5	4.4580	9.2210	0.0326
6	4.4898	9.4680	0.0312
7	4.5212	9.7560	0.0317
8	4.5534	10.0003	0.0331
9	4.5890	10.3283	0.0381
10	4.6245	10.6442	0.0330
11	4.6533	10.8921	0.0246
12	4.6816	11.1781	0.0321
13	4.7153	11.5487	0.0351
14	4.7480	11.9018	0.0305
15	4.7784	12.2565	0.0303
16	4.8095	12.6053	0.0320
17	4.8714	13.3924	0.0308
18	4.9031	13.8514	0.0326
19	4.9351	14.2510	0.0318
20	4.9664	14.7572	0.0308
21	4.9967	15.2151	0.0299
22	5.0262	15.7665	0.0289
23	5.0547	16.3217	0.0281
24	5.0828	16.9206	0.0281
25	5.1099	17.4394	0.0264
26	5.1359	18.0970	0.0255
27	5.1610	18.7843	0.0247
28	5.1852	19.5402	0.0238
29	5.2086	20.3050	0.0230
30	5.2311	21.2326	0.0220
31	5.2527	22.2640	0.0211
32	5.2733	23.4798	0.0201
33	5.2928	25.0205	0.0190
34	5.3111	27.0039	0.0177

TABLE III SMALL SAMPLE H = 0 K OE

	T	CM	DELTA T
35	5.3240	29.3691	0.0022
36	5.3261	29.6935	0.0019
37	5.3278	30.2641	0.0159
38	5.3280	30.5165	0.0019
39	5.3293	30.7376	0.0008
40	5.3301	30.4561	0.0008
41	5.3309	30.7576	0.0008
42	5.3317	31.2188	0.0008
43	5.3325	31.7637	0.0008
44	5.3332	31.6592	0.0008
45	5.3340	32.2676	0.0008
46	5.3348	32.6199	0.0008
47	5.3355	33.2143	0.0007
48	5.3362	33.1442	0.0007
49	5.3369	33.4755	0.0007
50	5.3376	33.5595	0.0007
51	5.3383	33.6466	0.0007
52	5.3391	33.2915	0.0007
53	5.3398	33.0552	0.0007
54	5.3406	32.7094	0.0007
55	5.3413	31.6212	0.0008
56	5.3421	31.0226	0.0008
57	5.3429	29.9923	0.0008
58	5.3446	27.2212	0.0009
59	5.3446	27.1197	0.0176
60	5.3455	25.4108	0.0009
61	5.3464	24.3489	0.0010
62	5.3475	22.5190	0.0011
63	5.3514	17.6781	0.0024
64	5.3539	16.3465	0.0025
65	5.3565	14.9530	0.0028
66	5.3594	13.5195	0.0030
67	5.3624	13.3581	0.0030
68	5.3654	12.8099	0.0031

TABLE III SMALL SAMPLE H = 0 K OE

	T	CM	DELTA T
69	5.3685	12.4001	0.0032
70	5.3705	12.7320	0.0344
71	5.3717	12.1233	0.0033
72	5.3750	11.8608	0.0033
73	5.3792	11.4586	0.0050
74	5.4086	10.0200	0.0418
75	5.4522	8.9103	0.0459
76	5.4995	8.2027	0.0488
77	5.5493	7.7364	0.0509
78	5.6010	7.3782	0.0525
79	5.6543	7.0520	0.0541
80	5.7091	6.8036	0.0554
81	5.7649	6.5977	0.0564

TABLE IV SMALL SAMPLE H = 1.04 K OE

	T	CM	DELTA T
1	5.3119	27.2489	0.0023
2	5.3154	27.8886	0.0045
3	5.3187	28.6296	0.0022
4	5.3209	28.9839	0.0022
5	5.3231	29.3574	0.0022
6	5.3252	30.0204	0.0021
7	5.3274	30.4739	0.0021
8	5.3294	31.2374	0.0020
9	5.3314	31.8848	0.0020
10	5.3334	32.3354	0.0020
11	5.3354	33.0310	0.0019
12	5.3373	33.3548	0.0019
13	5.3388	33.2265	0.0010
14	5.3398	32.3030	0.0010
15	5.3408	32.1893	0.0010
16	5.3423	29.7803	0.0021
17	5.3446	25.9300	0.0024
18	5.3473	21.6450	0.0029
19	5.3503	18.3428	0.0033
20	5.3539	15.8502	0.0038
21	5.3578	14.2608	0.0041
22	5.3621	13.3296	0.0044

TABLE V SMALL SAMPLE H = 5.00 K OE

	T	CM	DELTA T
1	5.2665	23.4512	0.0051
2	5.2715	24.0267	0.0050
3	5.2764	24.2618	0.0049
4	5.2813	24.8171	0.0048
5	5.2860	25.1037	0.0047
6	5.2906	25.6289	0.0046
7	5.2952	26.1695	0.0045
8	5.2997	26.8264	0.0044
9	5.3041	27.3527	0.0043
10	5.3084	28.0466	0.0043
11	5.3126	28.8133	0.0041
12	5.3140	29.4236	0.0021
13	5.3160	29.8844	0.0018
14	5.3166	29.9005	0.0040
15	5.3177	30.5267	0.0017
16	5.3194	31.0750	0.0017
17	5.3196	30.5599	0.0020
18	5.3210	30.8283	0.0009
19	5.3212	31.5556	0.0017
20	5.3219	31.3321	0.0008
21	5.3227	30.7842	0.0009
22	5.3228	32.2366	0.0016
23	5.3236	31.3946	0.0008
24	5.3244	31.6495	0.0008
25	5.3245	32.3277	0.0016
26	5.3252	32.2996	0.0008
27	5.3261	31.7134	0.0008
28	5.3261	32.5791	0.0016
29	5.3269	32.3618	0.0008
30	5.3277	32.5379	0.0008
31	5.3278	31.7277	0.0017
32	5.3285	33.1145	0.0008
33	5.3293	32.4100	0.0008
34	5.3294	31.0727	0.0017

TABLE VI SMALL SAMPLE H = 10.15 K OE

	T	CM	DELTA T
1	5.2414	24.0611	0.0049
2	5.2463	24.8910	0.0047
3	5.2509	25.3013	0.0046
4	5.2556	25.9405	0.0046
5	5.2600	26.5271	0.0044
6	5.2644	27.1937	0.0043
7	5.2687	27.9098	0.0042
8	5.2729	28.6698	0.0041
9	5.2769	29.6558	0.0040
10	5.2804	30.4203	0.0007
11	5.2808	30.6844	0.0039
12	5.2810	30.6487	0.0007
13	5.2817	30.8707	0.0007
14	5.2825	31.0102	0.0009
15	5.2834	31.0607	0.0009
16	5.2844	31.3624	0.0009
17	5.2853	31.5033	0.0009
18	5.2862	31.5430	0.0009
19	5.2871	31.4482	0.0009
20	5.2881	31.1852	0.0009
21	5.2890	30.9929	0.0009
22	5.2899	30.4943	0.0010
23	5.2909	30.1513	0.0010
24	5.2919	28.4591	0.0010
25	5.2923	28.9325	0.0041
26	5.2929	27.1150	0.0011
27	5.2940	25.9553	0.0011
28	5.2951	24.4889	0.0012
29	5.2963	22.9237	0.0012
30	5.2970	22.1591	0.0052
31	5.2976	21.5919	0.0013
32	5.3028	16.4954	0.0068
33	5.3103	13.6192	0.0080
34	5.3186	12.1701	0.0089

TABLE VII SMALL SAMPLE H = 18.98 K OE

	T	CM	DELTA T
1	5.0871	20.4291	0.0106
2	5.0972	22.1239	0.0098
3	5.1068	22.5743	0.0096
4	5.1163	23.1854	0.0094
5	5.1255	23.7479	0.0092
6	5.1345	24.6637	0.0089
7	5.1431	25.6052	0.0085
8	5.1514	26.8770	0.0082
9	5.1593	28.4281	0.0078
10	5.1668	30.0410	0.0074
11	5.1714	30.2102	0.0018
12	5.1732	29.5274	0.0019
13	5.1751	28.3601	0.0020
14	5.1772	25.4014	0.0022
15	5.1794	23.4370	0.0023
16	5.1819	20.5194	0.0026
17	5.1847	18.0519	0.0029
18	5.1931	13.7990	0.0148
19	5.2094	10.9580	0.0180
20	5.2279	10.0878	0.0193

APPENDIX A

TEMPERATURE CALIBRATION PROCEDURE

1. INTRODUCTION

The germanium resistor was calibrated from 1 K through 30 K using the helium vapor pressure temperature scale, T_{58}, below 4.2 K and using the pressure-temperature equation of state for a fixed number of moles of helium gas above 4.2 K. This appendix describes the procedure used to establish the temperature scale, the fitting of the data to an interpolation formula, and the experimental check on the accuracy of the temperature by measuring the specific heat of copper. Although, for the experiment discussed in this dissertation, such a broad range to temperatures was not needed, the calibration was carried out for other experiments which use the same calorimeter over a larger temperature range.

A calibration cryostat was constructed which consisted of a gas bulb and a vapor bulb machined into a copper cylinder. The resistors to be calibrated were inserted into holes in the copper. The temperature of the cylinder was controlled by providing it with thermal links to the liquid helium bath and to a heated shield surrounding it. The temperature of the shield was maintained with a Wheatstone-bridge controller similar to that used with the shield of the calorimeter. A schematic drawing of the system is given in Figure 13. The shield and outer vacuum can are not shown, nor is the vacuum

pumping line. The tubes shown run inside the vacuum line, so that they were not in contact with the liquid helium. The pressure of either bulb could be measured with a Texas Instruments quartz Bourdon tube gauge (maximum pressure: 300 Torr) or, at higher pressures, with a mercury manometer in conjunction with a cathetometer.

2. GAS BULB THERMOMETRY

The equation of state for n moles of a gas at pressure p, volume V, and temperature T is

$$n = \frac{pV}{RT+Bp} ,$$

where B is the virial coefficient (temperature dependent). The gas bulb thermometer is based on the fact that if V and n are known and if p is measured, T can be found since the virial coefficients are tabulated (Kilpatrick 55). This equation must be extended for a practical thermometer since not all parts of it are at the same temperature. For the thermometer employed, the equation of state can be written as

$$nR = p\left[\frac{V_{bulb}}{T+Bp/R} + \frac{V_{eq}}{T_{eq}} + \frac{V_{tubing}}{T_{tubing}} + \frac{V_{gauge}}{T_{gauge}}\right] . \qquad (1)$$

The term V_{eq}/T_{eq} accounts for the capillary tube, which has a temperature gradient along its length. An expression for this term will be derived later. The sum of the last three terms in equation (1) is designated D. The virial coefficients become small at high temperatures and are neglected in the calculation of D. If, at a known temperature T_o, the pressure is found to

be p_o, then

$$nR = p_o \left[\frac{V_{bulb}}{T_o + B_o p_o/R} + \left. \frac{V_{eq}}{T_{eq}} \right|_{T=T_o} + \frac{V_{tubing}}{T_{tubing}} + \frac{V_{gauge}}{T_{gauge}} \right] .$$

All the terms on the right can be measured or calculated. The bulb was filled at 77 K to about 770 Torr. At 4.2 K this produced a pressure of about 42 Torr, so that the digital reading on the Bourdon tube gauge was roughly ten times the temperature. Aside from this nicety, the filling pressure is not critical; what is critical is a careful measurement of p_o and T_o. T_o was determined from the vapor-bulb reading, and p_o from the Bourdon tube gauge. About 20 measurements of p_o and T_o were made at temperatures between 3.8 and 4.2 K and were averaged to find n. With n known, equation (1) could be solved for temperature in terms of pressure, were it not for the fact that B and V_{eq}/T_{eq} depend on temperature. However, as a first approximation, B and D can be neglected, and an approximate temperature is calculated from

$$T_1 = \frac{pV_{bulb}}{nR} .$$

This temperature is then used to enter a table of T vs B to find B and to calculate D. These are used to find a second approximation to T,

$$T_2 = p \left[\frac{V_{bulb}}{nR - pD(T_1)} - \frac{B(T_1)}{R} \right]$$

This value of T is used to find a better approximation for B and D. The process is repeated until successive values of T do not differ more than 5×10^{-5} K; this usually requires

about five iterations. V_{bulb} was assumed not to change over the temperature range of calibration; however, since it was measured at room temperature, a correction for its thermal contraction at 4 K was made. The sensitivity of the thermometer at 10 K was .1 mK/micron.

The gas in the capillary is not at a single temperature, but an effective temperature can be defined as follows:

$$V_{eq}/T_{eq} = \int_0^L \frac{A\ dy}{T}$$

where L is the length of the tube and A its cross-sectional area. This can be rewritten

$$\frac{V_{eq}}{T_{eq}} = A \int_T^{T_R} \frac{dT}{T\ dT/dy}$$

where T is the temperature at the bottom of the capillary and T_R is room temperature (300 K). Since $\dot{Q}/A = \varkappa(T)\ dT/dy$, where $\dot{Q}$ is a constant, and $\varkappa(T)$ is the thermal conductivity of the capillary, the equation becomes

$$V_{eq}/T_{eq} = \frac{A}{\dot{Q}/A} \int_T^{T_R} \frac{\varkappa(T)dT}{T}$$

Now $$\dot{Q}/A\ dy = \varkappa(T)dT$$

so $$\dot{Q}/A\ L = \int_T^{T_R} \varkappa(T)dT$$

hence $$V_{eq}/T_{eq} = V_{capillary}\left[\frac{\int_T^{T_R} \frac{\varkappa(T)dT}{T}}{\int_T^{T_R} \varkappa(T)dT}\right]$$

Up to 40 K the thermal conductivity of stainless steel can be expressed approximately as $\kappa(T) = .5T^{1.25}$. Using this fact, the integrals can be divided into two parts:

$$\frac{V_{eq}}{T_{eq}} = V_{capillary} \left[\frac{.5(40)^{1.25} - .5T^{1.25} + \int_{40}^{300} \frac{\kappa(T)dT}{T}}{\frac{.5(40)^{2.25}}{2.25} - \frac{.5T^{2.25}}{2.25} + \int_{40}^{300} \kappa(T)dT} \right]$$

The remaining integrals are found by numerical integration of the published thermal conductivity data (N.B.S. 54).

The gas bulb calibration points were taken with the helium bath at 4.2K. The shield was set at the desired temperature, and the controller regulated the temperature so that when the reistors reached equilibrium with the shield, no drift was noticeable. The pressure was read from the Bourdon tube gauge to $\pm$ 1 micron, and simultaneously the resistance was recorded. To make measurements of the number of moles, n, exchange gas was admitted into the vacuum space and helium was condensed in the vapor bath; after equilibrium, the gas bulb and the vapor bulb pressures were measured together. To obtain other points, the pressure above the bath was lowered from atmospheric pressure and held contant by a mechanical pressure regulator.

3. VAPOR BULB THERMOMETRY

The calibration points from 1 to 4 K were obtained by measuring the vapor pressure of a small amount of liquid helium condensed in the vapor bulb, which was in thermal equilibrium with the resistors. For pressures above 300 Torr a mercury

manometer was used, below 300 Torr the Bourdon tube gauge was used. The manometer heights were corrected to standard gravity and to 0 ^{o}C. Below 1.6 K it was necessary to apply a correction to the measured pressures to account for the thermomolecular pressure difference between the hotter gas at the gauge and the cold gas in the bulb, the gauge read a higher pressure than the true vapor pressure. This correction was calculated from published data (Roberts 56). At the lowest temperature the correction was about 5%. The corrected pressures were entered in the "1958 He^4 Scale of Temperature" (N.B.S. 60) to find the corresponding temperatures.

4. INTERPOLATION PROCEDURE

The final product of the calibration procedure outlined above was a collection of about 120 pairs of R and T. In order to obtain the temperature corresponding to an arbitrary resistance it is necessary to somehow interpolate between calibration points. Considerable effort was spent searching for the best method for doing this, since specific heat measurements of copper, to be described below, indicated that systematic errors would arise in calorimetry unless the interpolation procedure is treated properly.

If the calibration points had no experimental uncertainty, it would be a simple matter to interpolate using standard procedures. However one needs to smooth the calibration data; thus various function forms, $T = f(R)$, were fitted to the data using a least squares procedure.

No "simple" equation has been found relating temperature to reistance of germanium thermometers (Schriempf 66). A suitable criterion for a proper fit is one that shows no systematic trend in a plot of the deviation, $(T_{formula} - T_{data})$ vs T_{data}, where $T_{formula} = f(R_{data})$. One way found for achieving this is to determine a fit of the form

$$\frac{1}{T} = \sum_{i=1}^{6} A_i \, (\log R)^{i-1}$$

The deviations calculated from this fit appear roughly sinusodial. A smooth curve was drawn through the deviations and a table of ΔT vs T was constructed from the curve. The deviation corresponding to a given T is found by interpolation in the table, and the value of T given by the above equation is shifted by the deviation to get the final temperature.

Another approach is to simply use more and more coefficients in the polynomial. There is a limit to the success of this procedure caused by round-off error in the calculation, due to the limited number of significant digits carried by the computer. However a fairly satisfactory fit of the calibration data is given by

$$\ln T = \sum_{i=1}^{11} A_i (\ell n \, R)^{i-1} \qquad (2)$$

This form was used for the heat capacity calculations in this experiment. It was successful because the range of temperatures for which the equation applied was restricted to 2 to 10 K. Figure 14 is a plot of the difference between the measured temperature and that calculated from equation (2).

5. ACCURACY OF THE TEMPERATURE SCALE

It has been pointed out that heat capacity measurements on high-purity copper can be used to compare temperature scales and measurements techniques of various laboratories (Osborne 67). To this end a standard reference formula for the specific heat of copper was developed by fitting the data of several workers to the equation

$$C_{Cu} = \sum_{i=1}^{6} A_i T^{2i+1}. \qquad (3)$$

As a check on the accuracy of the temperature scale above 4 K, the specific heat of copper was measured and compared with values given by the reference equation. Two pieces were spark-cut from a single crystal having 99.9995% purity. Each piece had a mass of about 35 grams. The thermometer and heater were mounted on one piece and the other piece was glued below it. The heat capacity of this composite sample was measured. In a separate run the heat capacity of only one piece was measured. Subtraction of the two heat capacities eliminates the addenda contribution.

The measurements with the temperature scale used in this work deviate from the value predicted by this equation by less than .5% except above 19 K. It should be noted that two recent measurement (Ahlers 66) (Martin 66) also show about this same deviation, even though the reference equation is based partly on their data. Figure 15 is a plot of the deviation of the measured heat capacities from the values calculated using the reference formula. The points marked by $\underline{x}$ are calculated by correcting

the temperature given by equation (1) with the deviations, as discussed above. The points marked $\underline{0}$ are not corrected this way. This illustrates the systematic error that can arise from an unsatisfactory interpolation procedure.

In order to assess the accuracy of the temperature scale each calibration temperature was changed by x percent, and x was varied until the heat capacity deviation plot showed a systematic trend. This provides an idea as to how sensitive the copper heat capacity measurements are to errors in the temperature scale. The conclusion of this test is that between 4 K and 20 K the temperature scale is accurate to better than .5%. Or, worded more exactly, the scale agrees this well with the average of the scales of those workers whose data were used to determine the copper reference equation. Below 4 K the temperature scale accuracy is limited by the accuracy of the pressure measurements, the inherrent accuracy of the T_{58} scale, and the validity of correction made to account for the thermomolecular pressure difference. The mercury manometer readings were reproducible to $\pm$ .2 Torr, corresponding to an uncertainty in T of less than .5 millidegrees. Below 3 K the Bourdon tube gauge was used. Its calibration was carried out by the manufacturer, and is based on a traceable standard having an accuracy of $\pm$ .02 Torr. At the lowest temperature used, this corresponds to a temperature uncertainty of 1%. The thermomolecular correction is less than 5% of the temperature, and probably introduces negligible error. In sum then, the maximum uncertainty in the temperature scale is 1% at the low end, from 1 K to 2 K, and is less than .5% up to 20 K.

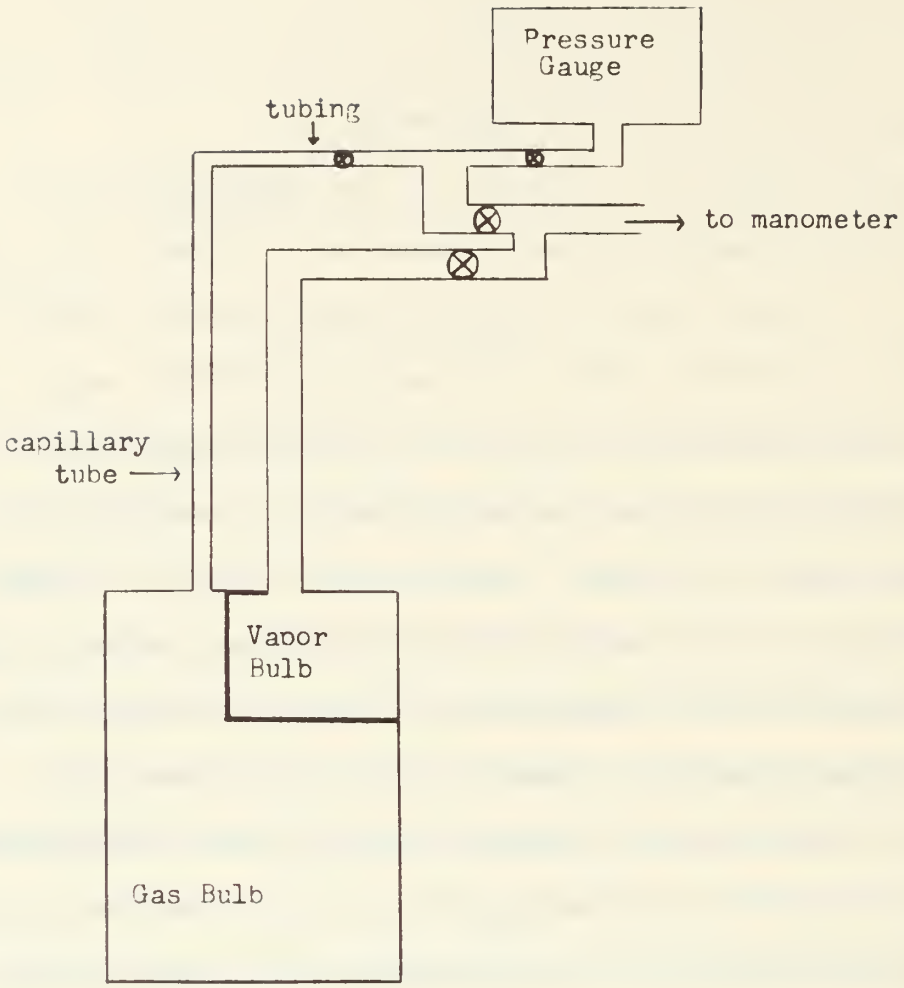

Figure 13: Calibration Cryostat

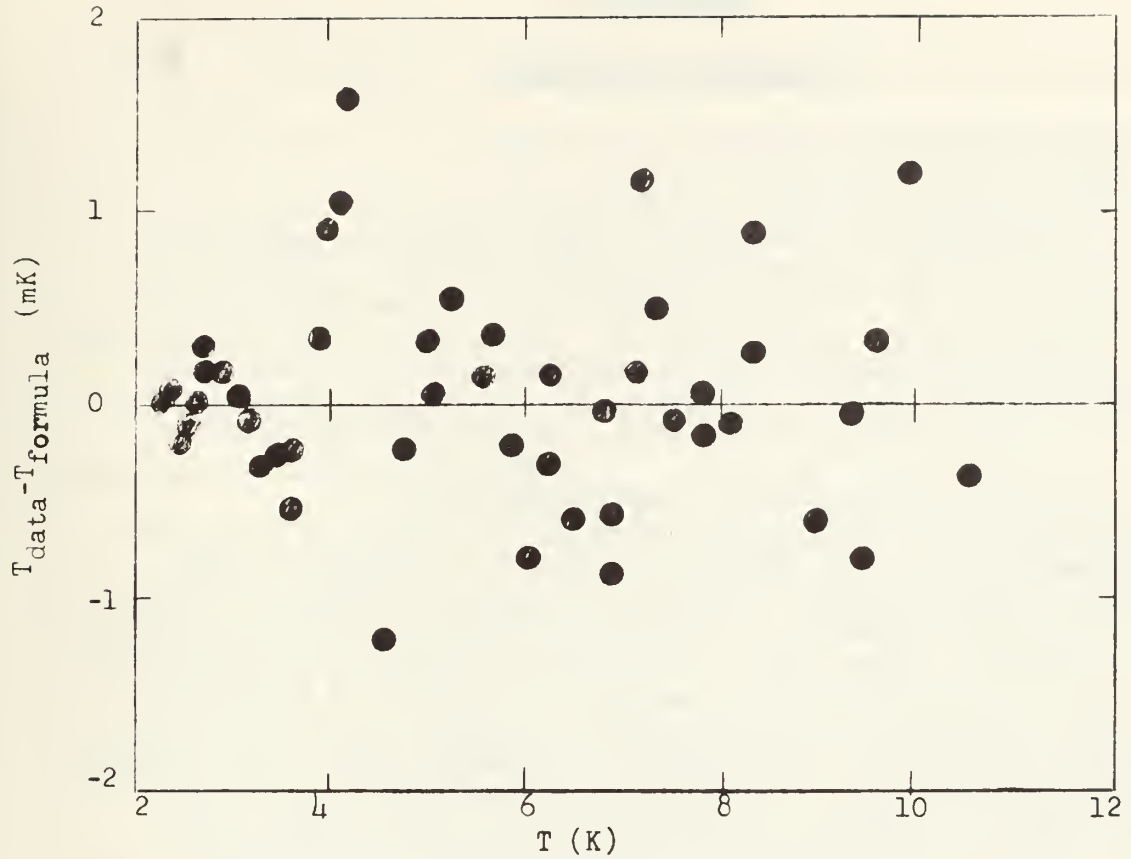

Figure 14: Deviations of data from Eq. 2.

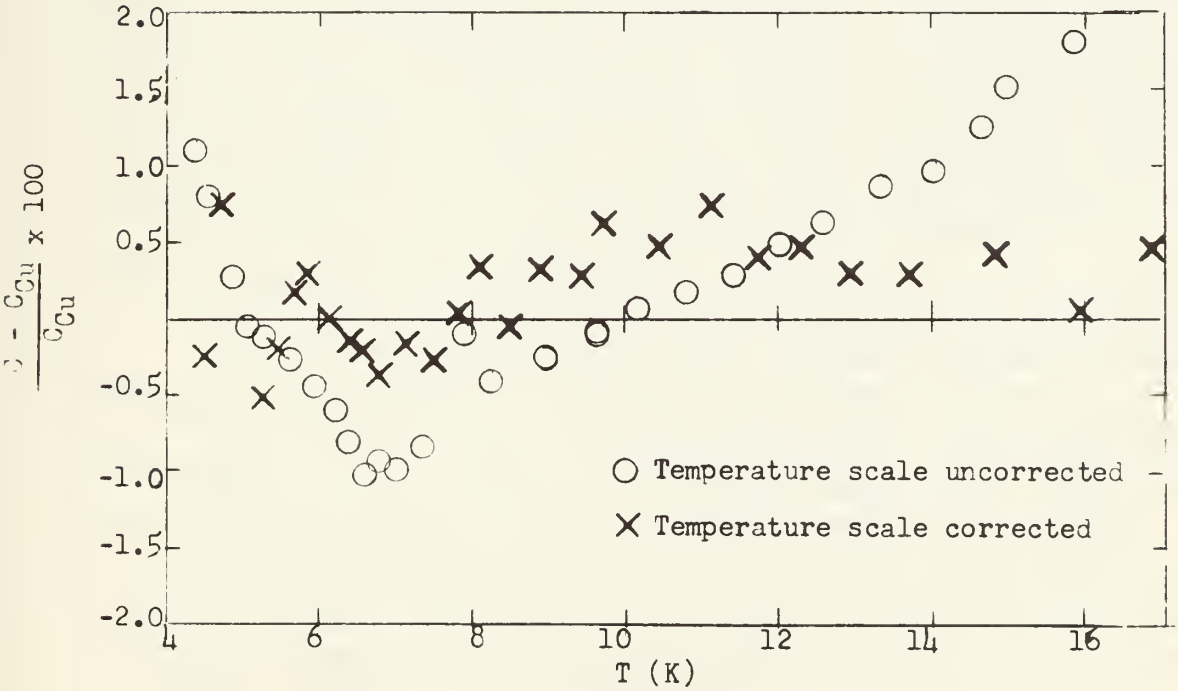

Figure 15: Deviations of copper heat capacity from Eq. 3.

APPENDIX B

ELECTRONIC CIRCUITS

1. MAGNET AND POWER SUPPLY

The superconducting magnet was made by Eastern Scientific Instruments. It is a solenoid, wound of niobium-titanium wire, which produces a field of 20 kilo-oersteds with a count of 23 amperes. It has been operated with currents as high as 29 amperes without destroying its superconductivity.

The magnet is 4 in. long and 2 7/8 in. in diameter, with a 1 5/8 in. bore diameter. It bolts to the outside of the brass can of the calorimeter and is immersed in the 4.2 K helium bath during the experiment. The magnet is equipped with a persistent-current switch. This is a superconducting shunt across the terminals of the magnet; wound around the shunt is a heater. When enough current is applied to the heater to raise the shunt's temperature above the transition temperature, the magnet terminals are effectively unshorted and connected to the power supply. In normal operation one heats the switch, establishes the desired field in the magnet by adjusting the current delivered by the power supply, then removes the heat from the persistent-current switch. The current last established in the magnet decays with a time constant L/r, where L is the inductance of the solenoid and r is the resistance of the connections between the shunt and the coil. In an experiment lasting several hours this decay of current is noticeable and the data must be

adjusted to correspond to a common field. To evaluate the time constant, a rotating-coil gaussmeter was placed outside the dewar near the position of the top of the magnet. At this position the fringe field was several-hundred gauss when the field at the center of the magnet was 10 kOe. The fringe field was measured at ½ hour time intervals for six hours. The field decayed approximately linearly with time, and L/r was evaluated to be 4×10^5 seconds, yielding $r = 4.6 \times 10^{-7}$ ohms.

The homogeneity of the magnet was measured using the magnetoresistance change of a germanium resistor which was moved vertically through the center of the coil. To do this, the jaws of the heat swtich were removed, leaving the shaft free to travel vertically when the bellows at the top of the cryostat was moved. The germanium resistor was mounted on the end of the shaft. Exchange gas was admitted into the sample space, so that, as the resistor was moved vertically any change in resistance was due to change in magnetic field, since the resistor's temperature quickly returned to that of the helium bath. Over a vertical range of $\pm$ 1 cm the field changed by .7%.

A controller and current regulator were constructed so that thecurrent to the solenoid could be increased or decreased at a steady rate. This control is important because superconducting magnets will go normal if the current is changed too rapidly. The maximum recommended rate of change of current for the magnet used was 1.6 amperes/second. The schematic diagram of the regulator and controller are shown in Fig. 16. This circuit is based

on one previously published (Fietz 65). The full magnet current flows through R_1, a .0477 ohm manganin strip mounted in an oil bath. The voltage drop across this resistor, R_1, is compared to that selected by the setting of R_2, which together with the 1.35 volt mercury cell, is also mounted in the oil bath. The difference between the two voltages is the error voltage which is amplified by A_1 and applied to the series transistor Q_1. This transistor adjusts the current to return the error voltage to zero. The magnet current is accurately determined by measuring the voltage across R_1 with a potentiometer. The additional circuit associated with amplifier A_2 serves to maintain dI/dt below a certain set point determined by the setting of R_3, R_4, and R_5. Their influences on dI/dt are coupled, but almost any combination of increase and decrease rates can be set. The terminal voltage, -LdI/dt, is monitored on the voltmeter, while the ammeter gives the approximate magnet current. A Kepco high-current power supply serves as the current source, although a 6 volt storage battery is sufficient. A No. 20 copper wire delivers the current to the solenoid in the dewar, and the return is made via the cryostat tubing. Considerable Joule heating is developed at the higher currents because of the use of such a small current lead. This results in rapid helium loss; however, such a situation exists only for a few minutes while the current is being established and measured, after which the magnet is put into the persistent mode. The terminal voltage and heater leads are .005 inch manganin wires.

2. SHIELD TEMPERATURE CONTROLLER

The calorimeter described in Section IV achieves adiabatic conditions because the sample is surrounded with a thermal shield which is maintained at the same temperature as the sample. The electronic circuit developed for controlling and setting the shield temperature is described in this section.

The initial controller which was constructed used a dc Wheatstone bridge to measure the shield temperature. The error voltage was amplified with a chopper amplifier and used to control power to the heater. This system had several disadvantages: Stray thermal voltages were developed and resulted in zero drift; the bridge dissipated about 5×10^{-6} watts in the shield resistor, and when attempting to reach temperatures near 1 K, this much power caused noticeable heating and limited the lowest temperature that could be reached.

A second controller was constructed using an ac bridge dissipating about 10^{-7} watts. The circuit was based on a liquid helium controller (Venegas 69); several modifications were made to improve the stability and sensitivity. A simplified version of the circuit is shown in Fig. 17. This does not show dc power circuits, switches, or other non-essential items.

A three-lead Wheatstone bridge operates at 318 Hz (1000/πHz); power is supplied to the bridge from an internal oscillator. Mounted on the shield are several carbon resistors, which can be selected for different temperature ranges. The off-balance bridge voltage is amplified by 50X by A_1, a balanced amplifies with an FET input. When the bridge is nulled, the output of A_1

is not zero because of reactive components in the bridge. However, as the error signal passes through minimum, the phase relative to the oscillator changes by 180^{o}. At the exact null point, the error voltage is 90^{o} out of phase with the oscillator. This phase change is detected and converted to a dc signal proportional to the error voltage.

A_2 is a narrow band-pass filter with a gain of one. It effectively rejects noise and passes only the error signal. The output of A_2 goes to A_3, whose gain can be varied from 4 to 400. A_4 is a follower used to provide low-impedance output to the chopper transistor, Q_1. A_7 is a sine wave to square wave converter which delivers switching pulses to Q_1. The pulses short the drain of Q_1 to ground each half cycle. Applied to the drain is the amplified 318 Hz error signal. This error signal is sampled for ½ cycle and integrated by a 5 KΩ, 10 μfd filter. If the error signal is 90^{o} out of phase with the oscillator (and therefore with the switching pulses), the input to A_5 is zero. If the bridge is unbalanced, a positive or negative voltage appears at the input of A_5. The output of A_5 varies from +5 through 0 to -5 volts as the phase of the error signal varies from 0^{o} to 180^{o} relative to the reference signal.

A_6 is a power amplifier which delivers a current to the shield heater proportional to its input. If the output of A_5 is zero, some quiescent current is required for the shield heater in order to maintain equilibrium. Therefore the output of A_5 is biased with a voltage divider circuit. If the output of A_5 goes

negative, A_6 delivers more current. If the error signal is positive, the heater current decreases and reaches zero when the voltage from A_5 cancels the bias voltage. A diode prevents A_6 from delivering current to the heater when the output of A_5 exceeds the magnitude of the bias voltage.

The gain of the controller can be adjusted in several places. The gain is set so that the system is nearly critically damped. If too much gain is used, the controller will run away with current oscillations growing in amplitude. In operation the decade box is set to correspond to the desired shield temperature. If this is warmer than the actual temperature, an increased heater current develops, the shield warms, usually overshooting the desired point. After a few oscillations (taking only a second or two) the current reaches a steady value, but the output of A_5 may not be zero. If not, the voltage divider is adjusted to bring it to zero.

The controller is capable of maintaining the shield temperature to within less than 2×10^{-4}K. During specific heat measurements for which maximum sample thermometer sensitivity was used, steady temperature drifts could be observed if the shield was misset by as little as 2Ω, corresponding to a temperature difference of 4×10^{-4}K. However when the shield was properly set, the sample would remain in equilibrium, indicating that the regulator was keeping the shield temperature constant to within $\pm 2 \times 10^{-4}$ K.

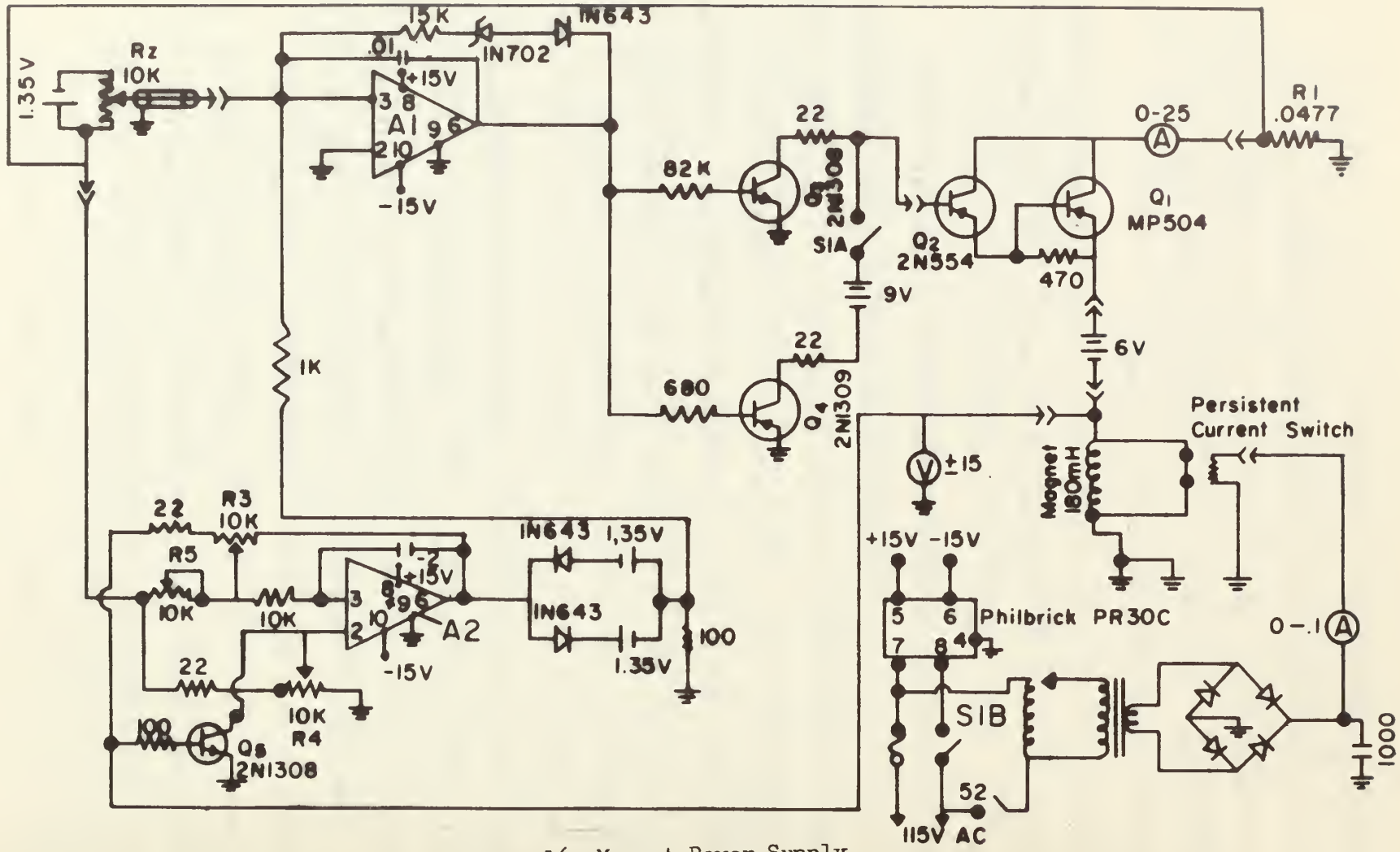

Figure 16: Magnet Power Supply

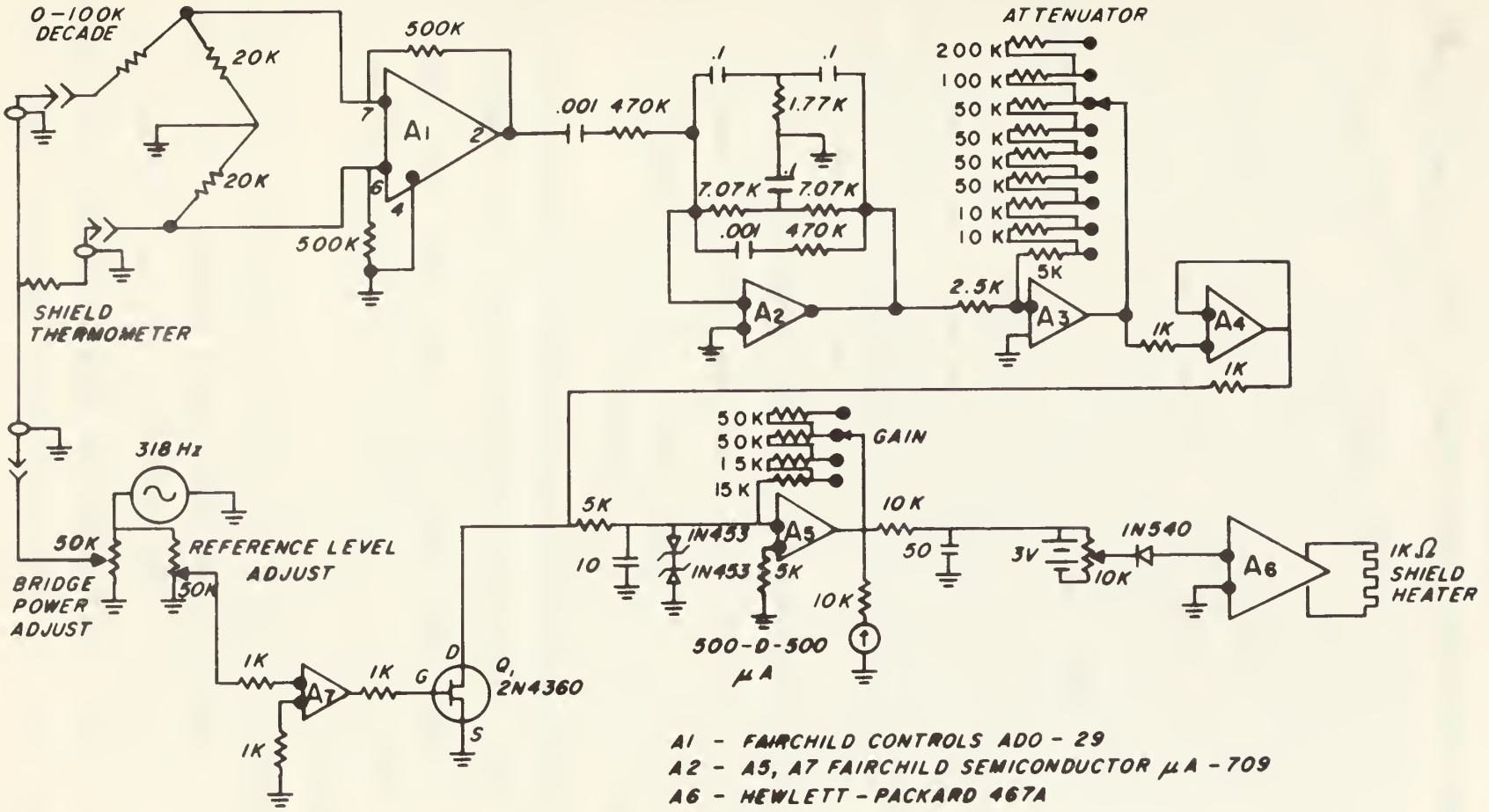

SHIELD TEMPERATURE CONTROLLER

Figure 17

APPENDIX C

HEAT CAPACITY OF MIXED NICKEL-COBALT CHLORIDE HEXAHYDRATE

This appendix describes measurements of the heat capacity of $Ni_xCo_{1-x}Cl_2 \cdot 6H_2O$ where x = .25 and .86. The purpose of these measurements was to determine if such a mixed salt would have a definite transition temperature, different from either the pure cobalt of nickel salt. NMR and susceptibility experiments had indicated that the Néel temperature was unique and varied between 2.29 K for x = 0 to 2.75 K for x = .5 (Robinson 65, 66).

$CoCl_2 \cdot 6H_2O$ has the same crystal structure as $NiCl_2 \cdot 6H_2O$; however, the Co ions have a spin of ½, and the easy axis is along the c crystal axis. A further difference is that the cobalt salt has a much higher anisotropy (Flippen 60). The mixed crystals were found to have the same lattice parameters with x = 0 as with x = .5 indicating that the mixed crystals are isomorphic to both the pure Co and Ni crystals.

The heat capacity measurements were made by the author and W. Reese in 1966. An entirely different cryostat and temperature calibration procedure than described in this thesis were used (Tucker 66). There was an uncertainty in the temperature scale of about .03 K.

About 5 grams of small mixed crystals were placed in a copper can on which a heater and thermometer were mounted. The can was filled with silicon oil to provide thermal contact between the crystals and the can. No attempt was made to evaluate the addenda; it is estimated that it contributes about 1-2% of the total near the maximum.

The data for x = .25 are plotted in Fig. 18. The shape of the peak is similar to that observed in the pure cobalt salt (Skalyo 64); however, it is broader, probably because the sample was polycrystalline. The sample with x = .86 was not investigated as throughly. Its heat capacity has a peak at 3.9 K.

While these experiments are not conclusive, it appears that large concentrations of nickel in the cobalt salt, or vice versa, give rise to an antiferromagnetic transition at a temperature intermediate between the Néel temperature of the two pure salts. Further research on the sublattice magnetization direction and careful measurements of the specific heat of mixed single crystals would be useful in understanding these transitions.

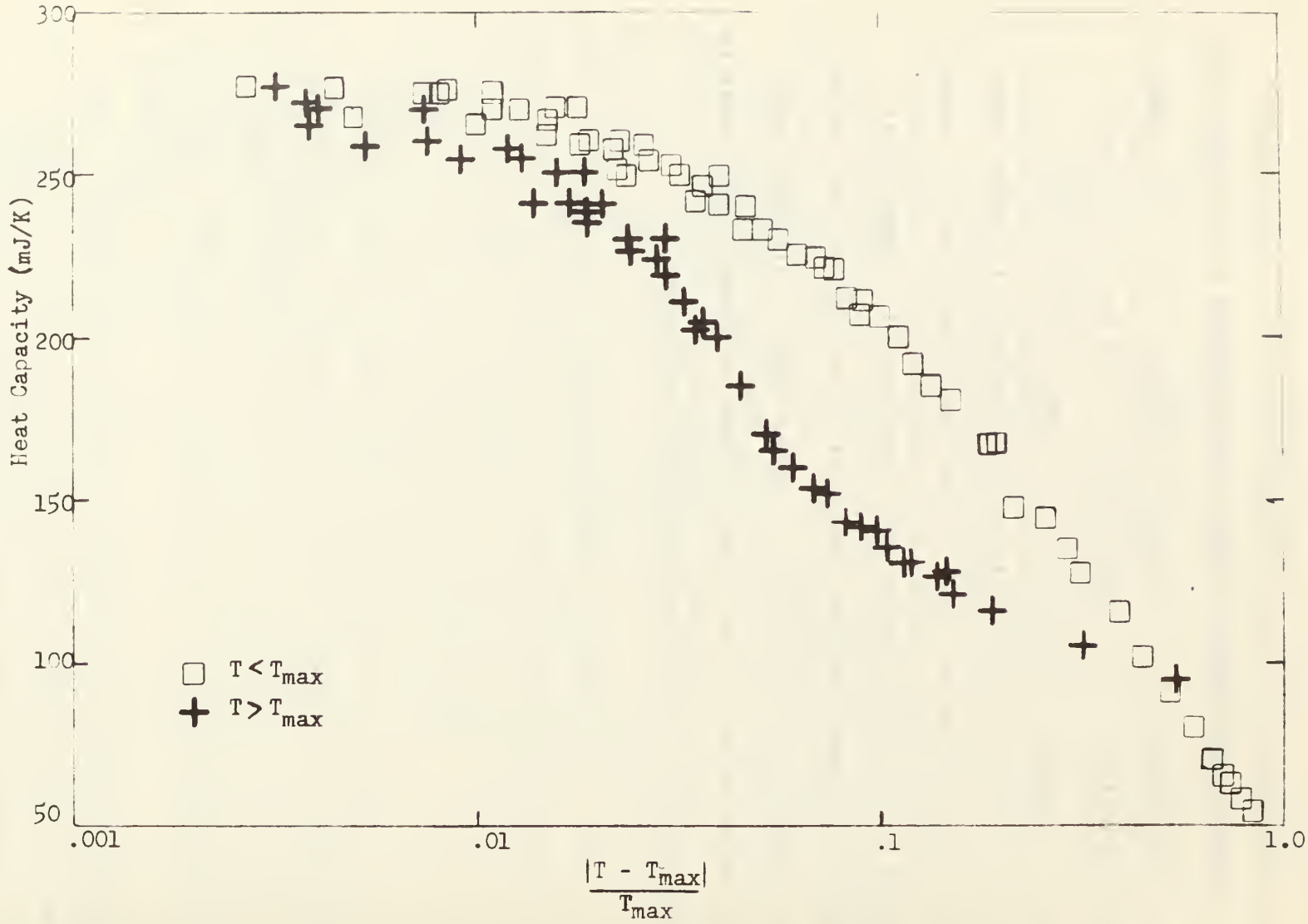

Figure 18: Heat capacity of $Ni_{.25}Cl_{.75}\ 6H_2O$, T_{max}=2.45 K

BIBLIOGRAPHY

Ahlers, G., "Heat Capacity of Copper," The Review of Scientific Instruments, v. 37, p. 477-480, April 1966.

Anderson, P.W., "Theory of Exchange in Insulators," Solid State Physics, Volume 14, edited by Seitz, F. and Turnbull, D., p. 99-214, Academic Press, 1963.

Anderson, P.S., "Exchange in Insulators: Superexchange, Direct Exchange, and Double Exchange," Magnetism, Volume I, edited by Rado, G.T. and Suhl, H., p. 25-83, Academic Press, 1963.

Baker, G.A., "Further Applications of the Padé Approximate Method to the Ising and Heisenberg Models," The Physical Review, v. 129, p. 99-102, 1 January 1963.

Belanger, B.C., "The Behavior of Carbon Resistor Thermometers in Magnetic Fields up to 100 kOe in the Pumped Liquid Helium and Hydrogen Temperature Ranges," The Review of Scientific Instruments, v. 40, p. 1082-1085, August, 1969.

Bienenstock, A., "Variation of the Critical Temperature of Ising Antiferromagnets with Applied Magnetic Field," Journal of Applied Physics, v. 37, p. 1459-1461, 1 March 1966.

Cadieu, F.J. and Douglas, D.H., "Effects of Impurities on Higher Order Phase Transitions," Physical Review Letters, v. 21, p. 680-682, 2 September 1968.

Clement, J.R., and Quinnell, E.H., "The Low Temperature Characteristics of Carbon Composition Thermometers," The Review of Scientific Instruments, v. 23, p. 213-216, May 1952.

Date, M. and Motokawa, M., "Antiferomagnetic Resonance in $NiCl_2 \cdot 6H_2O$," Journal of the Physical Society of Japan, v. 22, p. 165-173, January 1967.

Dixon, G.S., and Rives, J.E., "High Resolution Specific Heat Measurements on $MnCl_2 \cdot 4H_2O$ Near its Néel Temperature," The Physical Review, v. 177, p. 871-877, 10 January 1969.

Domb, C., and Miedema, A.R., "Magnetic Transitions," Progress in Low Temperature Physics, p. 296-343, 1964.

Fietz, W.A., "Stable Current Regulator for Superconducting Solenoids," The Review of Scientific Instruments, v. 36, p. 1306-1309, September 1965.

Fisher, M.E., "Lattice Statistics in a Magnetic Field I. A Two-Dimensional Super-exchange Antiferromagnet," Proceedings of the Royal Society, v. A254, p. 66-85, 19 January 1960.

Fisher, M.E., "The Nature of Critical Points," Lectures in Theoretical Physics, v. VII C, p. 1-159, The University of Colorado Press, 1965.

Fisher, M.E., and Ferdinand, A.E., "Interfacial, Boundary, and Size Effects at Critical Points," Physical Review Letters, v. 19, p. 169-172, 24 July 1967.

Ginzburg, V.L., and Pitaevskii, L.P., "On The Theory of Superfluidity," Translation in Soviet Physics JETP, v. 34 (7), p. 858-861.

Groth, P., Chemische Kristallographie, I Teil, p. 247, Engelmann, 1906.

Haseda, T., and Date, M., "The Paramagnetic Susceptibility of Some Nickel Salts," Journal of the Physical Society of Japan, v. 13, p. 175-178, February 1958.

Haseda, T., Kobayashi, H. and Date, M., "Paramagnetic Susceptibility of Single Crystals of Some Nickel Salts," Journal of the Physical Society of Japan, v. 14, p. 1724-1727, December 1959.

Flippen, R.B., and Friedberg, S.A.,"Magnetic Susceptibilities of Single Crystal $NiCl_2 \cdot 6H_2O$ at Low Temperatures," Journal of Applied Physics, Supplement to v. 31, p. 3385-3395, May, 1960.

Kilpatrick, J.E., Keller, W.E., and Hammel, E.F., "Second Virial Coefficients of Helium from the Exp-Six Potential," The Physical Review, v. 97, p. 9-12, 1 January 1955.

Kleinberg, R., "Magnetic Structure of $NiCl_2 \cdot 6H_2O$," Journal of Applied Physics, v. 38, p. 1453-1454, 1 March 1967.

Kleinberg, R., "Crystal Structure of $NiCl_2 \cdot 6H_2O$ at Room Temperature and 4.2 °K by Neutron Diffraction," paper presented at American Physical Society Meeting, Philadelphia, March 1969.

Maki, K., and Guyon, E., "Effects de Taille dans L'Hélium Superfluide II. Étude par une Methode de Fonctionnelle," Le Journal de Physique, v. 30, p. 63-70, January 1969.

McElearney, J., Low Temperature Adiabatic Studies of Magnetic Phase Boundaries in Antiferromagnets, Ph.D. Thesis, Michigan State University, 1968.

Martin, D.L., "Specific Heats of Copper, Silver, and Gold Below 30°K," The Physical Review, v. 141, p. 576-582, January 1966.

Mizuno, J., "The Crystal Structure of Nickel Chloride Hexahydrate, $NiCl_2 \cdot 6H_2O$," Journal of the Physical Society of Japan, v. 16, p. 1574-1580, August 1961.

Nagamiya, T., Yosida, K. and Kubo, R., "Antiferromagnetism," Advances in Physics, v. 4, p. 2-112, January 1955.

National Bureau of Standards Circular 556, Thermal Conductivity of Metals and Alloys at Low Temperatures, by Powell, R.L. and Blanpied, W.A., p. 43, September 1, 1954.

National Bureau of Standards Monograph 10, The 1958 He^4 Scale of Temperatures, by Brickwedde, R.G., and others, June 17, 1960.

Osborne, D.W., Flotow, H.E. and Schreiner, F., "Calibration and Use of Germanium Resistance Thermometers for Precise Heat Capacity Measurements from 1 to 25°K. High Purity Copper for Interlaboratory Heat Capacity Comparisons," The Review of Scientific Instruments, v. 38, p. 159-168, February 1967.

Onsager, L., "Crystal Statistics. I. A Two-Dimensional Model with an Order-Disorder Transition," The Physical Review, v. 65, p. 117-149, February 1944.

Roberts, T.R., and Sydoriak, S.G., "Thermomolcular Pressure Ratios for He^3 and He^4," The Physical Review, v. 102, p. 304-308, April 15, 1956.

Robinson, W.A., and Simmons, W.W., "Néel Temperature and Magnetic Susceptibilities of Mixed Hydrated Nickel-Cobalt Chlorides," Technical Report 9990-7179-R0000, TRW Systems, December 1965.

Robinson, W.A., and Simmons, W.W., "Chloride NQR in $NiCl_2 \cdot 6H_2O$-$CoCl_2 \cdot 6H_2O$ Mixed Crystals," Paper presented at American Physical Society Meeting, March 1966.

Robinson, W.K., and Friedberg, S.A., "Specific Heats of $NiCl_2 \cdot 6H_2O$&between 1.4° and 20°K," Physical Review, v.117, p. 402-408, January 15, 1960.

Sawatzky, E., and Bloom, M., "Proton Magnetic Resonance in Paramagnetic and Antiferromagnetic $CoCl_2 \cdot 6H_2O$," Canadian Journal of Physics, v. 42, p. 657-677, April 1964.

Schriempf, J.T., "A Comparison of Equations for Germanium Resistor Thermometry in the 2 - 20°K Range, Cryogenics, v. 6, p. 362-363, December 1966.

Skalyo, J., and Friedberg, S.A., "Heat Capacity of the Antiferromagnet $CoCl_2 \cdot 6H_2O$ Near its Néel Point," Physical Review Letters, v. 13, p. 133-135, 27 July, 1964.

Spence, R.D., Middents, P., El Saffer, Z., and Kleinberg, R., "A Proton Resonance Study of the Magnetic Structure of Antiferromagnetic $CoCl_2 \cdot 6H_2O$, $CoBr_2 \cdot 6H_2O$, $NiCl_2 \cdot 6H_2O$, and $NiBr_2 \cdot 6H_2O$," Journal of Applied Physics, v. 35, p. 854, March 1964.

Teaney, D.T., "Specific-Heat Singularity in MnF_2," Physical Review Letters, v. 14, p. 898-899, 31 May 1965.

Teaney, D.T., van der Hoeven, B.J.C., and Moruzzi, V.L., "Singular Behavior of a Ferromagnet in Nonzero Field," Physical Review Letters, v. 20, p. 722-724, 1 April 1968.

Tucker, J.E., Heat Capacity Measurements on Polyethylene in the Temperature Range 2.4 to 30°K, Ph.D. Thesis, Naval Postgraduate School, 1966.

van der Hoeven, B.J.C., Teaney, D.T., and Moruzzi, V.L., "Magnetic Equation of State and Specific Heat of EuS Near the Curie Point," Physical Review Letters, v. 20, p. 719-721, 1 April 1968.

Venegas, C.M., and Finegold, L., "Simple, Inexpensive Liquid Helium Temperature Controller, Using Integrated Semiconductor Circuits," The Review of Scientific Instruments, v. 40, p. 159-162, January 1969.

INITIAL DISTRIBUTION LIST

		No. Copies
1.	Defense Documentation Center Cameron Station Alexandria, Virginia 22314	20
2.	Library, Code 0212 Naval Postgraduate School Monterey, California 93940	2
3.	Chairman, Department of Physics Naval Postgraduate School Monterey, California 93940	2
4.	Assoc. Prof. William Reese Department of Physics Code 61Rc Naval Postgraduate School Monterey, California 93940	5
5.	William L. Johnson Department of Physics Code 61Jb Naval Postgraduate School Monterey, California 93940	5

Unclassified
Security Classification

DOCUMENT CONTROL DATA - R & D

(Security classification of title, body of abstract and indexing annotation must be entered when the overall report is classified)

1. ORIGINATING ACTIVITY *(Corporate author)*
Naval Postgraduate School
Monterey, California 93940

2a. REPORT SECURITY CLASSIFICATION
Unclassified

2b. GROUP

3. REPORT TITLE
Calorimetric Investigation of the Antiferromagnetic Transition in $NiCl_2 \cdot 6H_2O$

4. DESCRIPTIVE NOTES *(Type of report and, inclusive dates)*
Ph.D. Dissertation, December 1969

5. AUTHOR(S) *(First name, middle initial, last name)*
William Lewis Johnson

6. REPORT DATE	7a. TOTAL NO. OF PAGES	7b. NO. OF REFS
December 1969	106	45

8a. CONTRACT OR GRANT NO.	9a. ORIGINATOR'S REPORT NUMBER(S)
b. PROJECT NO. N/A	N/A
c.	9b. OTHER REPORT NO(S) *(Any other numbers that may be assigned this report)*
d.	N/A

10. DISTRIBUTION STATEMENT
This document has been approved for public release and sale; its distribution is unlimited.

11. SUPPLEMENTARY NOTES	12. SPONSORING MILITARY ACTIVITY
N/A	Naval Postgraduate School Monterey, California 93940

13. ABSTRACT

The results of measurements of the specific heat of nickel chloride hexahydrate in zero and various applied fields are presented. The specific heats of two single-crystal samples were determined in zero field between 4.3 and 5.8 K with temperature resolution of 10^{-6}K. The functional form of the specific heat near the Néel temperature is determined and compared with theoretical predictions. The specific heat maximum of both crystals is found to be rounded over several millidegrees. This non-ideal behavior is analyzed in terms of a complex transition temperature, the imaginary part of which is related to crystalline imperfections. Using data outside the rounded region, it is concluded that the Néel temperature of a perfect crystal would be $5.3475 \pm .001$ K. The effect of magnetic fields applied along the easy axis on the specific heat peak was investigated. The peak was found to be slightly broadened by the field, and occurred at lower temperatures. The boundary between antiferromagnetic and paramagnetic phases was determined for fields to 20 kilo-oersteds.

DD FORM 1 NOV 65 1473 (PAGE 1)
S/N 0101-807-6811

Unclassified
Security Classification

A-31408

14 KEY WORDS	LINK A		LINK B		LINK C	
	ROLE	WT	ROLE	WT	ROLE	WT
Antiferromagnets						
Phase Transition						
Specific Heat						
Heat Capacity						
Low-temperature Thermal Properties						
Nickel Chloride						